scientific reports

OPEN

Seismic wave reflection characteristics and wave-induced fluid flow in unsaturated porous solid

Manjeet Kumari[1], Pradeep Kaswan[2], Manjeet Kumar[2], Roland W. Lewis[3], Hakan F. Oztop[4,5,6], Nirmal Singh[7], Adebowale Martins Obalalu[8], Mukesh Pushkarna[9] & Milkias Berhanu[10]✉

This study examines the characteristics of seismic wave reflection and wave-induced fluid flow (WIFF) in an unsaturated porous solid half-space confined beneath an impermeable plane surface. We first present the field equations and constitutive relations for partially saturated porous media. Next, we solve these equations in terms of the Christoffel equations, thereby addressing the propagation of a four-plane harmonic wave. These waves propagate as inhomogeneous waves at stress-free, impermeable boundary surfaces due to the medium's dissipative properties. Furthermore, we compute the reflection coefficients from stress-free impervious boundary surfaces at arbitrary angles. The incidence of the P_1/SV wave generates four reflected waves. The calculation of theoretical formulations for reflection coefficients involves a set of four non-homogeneous linear equations derived from boundary conditions. Subsequently, these reflection coefficients are utilized to calculate the WIFF and the partitioning of incident energy at the impervious boundary of the porous solid. A numerical example is considered to investigate the effects of wave frequency, incidence direction, and elastic parameters such as porosity, inclusion radius, and liquid saturation on energy partitioning and wave-induced fluid flow. The conservation of incident energy has been confirmed at every angle of incidence. The numerical results demonstrate a significant dependence of energy shares of distinct reflected waves on the incident direction, saturation, porosity, inclusion radius, wave frequency, and WIFF. This theoretical study serves as a valuable tool for subsurface reservoir characterization, with applications in hydrocarbon exploration, CO_2 sequestration monitoring, and other geological engineering fields.

Keywords Partially saturated, Porous, Wave-induced fluid flow, Inhomogeneous, Reflection

List of symbols

η_{fm}	Viscosity of $\mathrm{mth}(=1,\ 2)$ fluid phase
κ	Intrinsic permeability of host medium
ϕ	Porosity of the porous material
ϕ_{10}	Partial porosity host medium
ϕ_{10}	Partial porosity inclusion
ϕ_m	Porosity occupied by $\mathrm{mth}(=1,\ 2)$ fluid
ρ	Mass coefficients

[1]Department of Mathematics, M P College for Women, Mandi Dabwali, Sirsa, Haryana 125104, India. [2]Department of Mathematics, Dr. B R Ambedkar Government College, Dabwali, Sirsa, Haryana 125104, India. [3]Department of Civil Engineering, Swansea University, Swansea, UK. [4]Department of Mechanical Engineering, Technology Faculty, Fırat University, Elazig, Turkey. [5]Department of Medical Research, China Medical University Hospital, Taichung, Taiwan. [6]University Centre for Research & Development, Chandigarh University, Mohali, Punjab 140413, India. [7]Department of Mathematics, NSCBM Government Degree College, Hamirpur, Himachal Pradesh 177005, India. [8]Department of Mathematics and Statistics, Kwara State University, Malete, Nigeria. [9]Department of Electrical Engineering, GLA University Mathura, Mathura, India. [10]Department of Electrical and Computer Engineering, College of Engineering, Sustainable Energy Center of Excellency, Addis Ababa Science and Technology University, Addis Ababa, Ethiopia. ✉email: milkias.berhanu@aastu.edu.et

ρ_{fm}	Density of $\mathrm{mth}(=1,\ 2)$ fluid phase
$\sigma^{(j)}_{(0)}$	Components of the stress of $\mathrm{jth}(=1,\ 2)$ fluid phase
σ_{ij}	Components of the stress of solid phase
A	Capillary pressure amplitude coefficient
K_m	Bulk modulus of matrix
K_s	Bulk modulus of minerals
K_{fm}	Bulk modulus of $\mathrm{mth}(=1,\ 2)$ fluid phase
k_{fm}	Relative permeability of $\mathrm{mth}(=1,\ 2)$ fluid phase
m	Friction coefficients
N_m	Shear modulus of matrix
R_0	Radius of inclusion
S_j	Saturation of $\mathrm{jth}(=1,\ 2)$ fluid
S_{rm}	Residual saturation of $\mathrm{mth}(=1,\ 2)$ fluid phase
u_i	Displacement components of solid phase
$U_i^{(j)}$	Displacement components of of $\mathrm{jth}(=1,\ 2)$ fluid phase

The impact of reflection dispersion resulting from mesoscopic flow is significant and deserves attention, as conventional quantitative seismic interpretations can be misleading. Local flow-induced phase variations may introduce uncertainty in the seismic imaging of geological formations. The implications of reflection dispersion for characterizing heterogeneous reservoir rocks are promising, suggesting the potential to utilize frequency-dependent seismic attributes to uncover geological heterogeneity and fluid mobility characteristics. In various geological contexts, multiple distinct fluids can partially saturate porous rocks. In the upper sections of gas-capped reservoirs, gas, oil, and brine often coexist within the available pore space. Additionally, contaminants can infiltrate subterranean aquifers. Groundwater levels may fluctuate due to earthquakes, and subsequent aftershocks are associated with changes in pore fluid distribution. To effectively interpret seismic data for hydrocarbon detection, monitor saltwater intrusion into groundwater aquifers, or analyze reported earthquake waveforms, it is essential to understand how partial fluid saturation influences elastic wave propagation.

The comprehensive model for elastic wave propagation in porous, fluid-saturated media is described by Biot's equations, as outlined in[1–3]. These equations were formulated using the Lagrangian approach, which defines generalized coordinates based on the average displacements of both solid and fluid components. A dissipation function, dependent on the relative velocity between the solid and liquid phases, was integrated into this framework. In the static or low-frequency limit, Biot's equations reduce to Gassmann's equation[4], which determines the undrained static bulk modulus of porous materials by considering the properties of the dry framework and the saturating fluid. Both sets of equations assume a single Newtonian fluid (liquid or gas) saturating the porous medium. Subsequent studies have reproduced Biot's equations using alternative mathematical methods, including volume averaging techniques proposed by Pride et al.[5] and homogenization approaches for periodic structures[6–8]. These methods yield similar macroscopic equations, thereby validating Biot's original formulation. Recently, numerous fluid flow problems have been addressed by researchers and published in the open literature (see Babu et al.[9], Zhao et al.[10], Kommaddi et al.[11], Kodi et al.[12] -[13]).

Biot's theory, however, is limited to fully saturated media containing a single fluid. Modeling wave propagation in porous materials with multiple immiscible fluids presents significant challenges. Immiscibility refers to the property of fluids that prevents them from mixing, resulting in distinct boundaries between different fluids[14]. Porous rock formations, such as sandstone, limestone, and shale, can be saturated with various pore fluids, including gas, water, and oil. Since the 1960s, researchers have increasingly focused on elastic wave propagation in partially saturated media. Brutsaert[15] pioneered the extension of Biot's theory by employing mixture theory to account for the effects of two immiscible pore fluids on elastic wave propagation. This mixture theory approach, initially developed for two-fluid systems, has since been refined and expanded by numerous researchers (Brutsaert and Luthin[16]; Bedford and Drumheller[17]; Garg and Nayfeh[18]; Berryman et al.[19]; Santos et al.[20,21]; Corapcioglu and Tuncay[22]; Tuncay and Corapcioglu[23]; Wei and Muraleethara[24,25]; Hanyga[26]; Lu and Hanyga[27]; Lo[28]; Lo et al.[29]). In materials with voids occupied by two immiscible fluids, capillary forces become significant, leading to the prediction of a third compressional wave, specifically a second slow wave. These slow waves are present and attenuate the primary compressional wave through mode conversion. Multiphase poroelasticity theory reveals the existence of four elastic wave modes: three longitudinal waves and one shear wave, which are solutions to coupled differential equations of motion. The extensive analysis of wave propagation in porous materials containing multiphase fluids is credited to Corapcioglu and Tuncay[22] as well as Tuncay and Corapcioglu[23]. Lo et al.[30] formulated a complex set of interconnected partial differential equations to elucidate the propagation of dilatational waves in an elastic porous medium containing two immiscible fluids. These equations illustrate the behavior of acoustic waves in porous media with multiple fluid phases, enhanced by the fundamental principles of poroelasticity. Lo et al.[31] analyzed various types of dilatory motion by determining the normal coordinates for the three longitudinal waves. They derived equations that describe the relationship between the modes of motion and the saturation level. The hydrologic models of subsurface multiphase flow discussed earlier do not account for the impact of viscous resistance caused by the relative velocity of two adjacent fluids on the behavior of elastic waves in partially saturated porous media. Lo et al.[32] introduced a mathematical model that utilizes continuous mixture theory to address the viscous cross-coupling between two immiscible pore fluids. Consequently, all the models mentioned above can be derived as specific instances of this framework. Furthermore, if only one fluid is present in the medium, this model can be simplified to Biot's theory[1,2]. The mathematical model established by Arora et al.[33] examined wave propagation in a porous medium composed of two solids saturated with two immiscible fluids. The equations for complementary energy and the linear stress-strain relationships of the medium were developed using the concept of virtual complementary work. The Lagrangian motion equation generates a network of interrelated partial differential equations. Xiong et al.[34] analytically demonstrated that the model presented by Tuncay and Corapcioglu[23], utilizing the volume averaging method, may exhibit instability due to potential structural deficiencies in the wave equations. To address this issue, they established an innovative mathematical framework for wave propagation in partially saturated porous media based on their findings.Wang et al.[35] provide a modeling framework designed to simulate wave propagation in heterogeneous, partially saturated porothermoelastic materials. Sun et al.[36] presented wave equations for the Biot-patchy-squirt mechanism based on Lagrangian equations, mass conservation equations, and constitutive equations for double-porosity media. For partially saturated porous media, Solazzi et al.[37] developed an analytical model to calculate frequency-dependent relative permeability functions that account for viscous coupling effects. Deng et al.[38] established a methodology for assessing compaction and monitoring liquefiable soils in mine dumps with fluctuating saturation due to rising groundwater levels. The behavior of waves propagating in non-isothermal poroelastic materials saturated with two-phase fluids was described by a model presented by Santos et al.[39]. The dynamic differential equations incorporate poroelasticity and heat equations, which integrate the solid, fluid, and thermal fields through coupling terms. A plane wave analysis demonstrated that five distinct waves could propagate.

As seismic waves propagate through rocks, they create pressure differentials at various depths, inducing fluid motion. Wave-Induced Fluid Flow (WIFF) can be classified into three categories based on pressure gradient length scales: mesoscopic, global, and squirt flows. The relationship between wave dispersion and attenuation across a broad frequency spectrum is closely linked to the WIFF process. Developing theoretical models that connect multiscale WIFF with wave propagation may enable the establishment of quantitative characteristics and precise assessments of reservoirs. The WIFF induced by waves is a primary factor contributing to wave dispersion and attenuation, which is significantly influenced by pore structure, fluid properties, and rock type (Yao et al.[40]; Müller et al.[41]; Quintal et al.[42]; Khalid and Ahmed[43]). However, this critical mechanism is not considered in all the multiphase fluid models mentioned in the previous paragraph. Recognizing the significance of this mechanism, Shi et al.[44] introduced a rock seismic model that incorporates three wave-induced fluid flow (WIFF) processes at varying scales, from the size of pores to the wavelength. The model examines a three-phase porous medium that includes two immiscible fluids within its pores. Shi et al.[44] focused exclusively on the dispersion and attenuation of seismic waves-specifically, velocity and attenuation-resulting from WIFF in unsaturated porous media. Reflected seismic data is frequently employed in exploratory geophysics to evaluate rock properties such as porosity, fluid saturation, and permeability. Therefore, we extend the study by Shi et al.[44] to investigate wave-induced fluid dynamics and the characteristics of seismic wave reflection in partially saturated porous media. First, we present a mathematical model for the propagation of a planar harmonic wave. The solution to the Christoffel equation reveals the presence of four waves in the medium: three compressional waves and one shear wave. Additionally, we calculate the poroelastic reflection coefficients from the boundary surface of sealed holes in porous media at various angles. These poroelastic reflection coefficients are subsequently utilized to compute wave-induced fluid flow and to separate energy contributions. We examine the behavior of energy share curves and wave-induced fluid flow (WIFF) curves at different frequencies of incident waves and angles of incidence, as well as elastic parameters such as porosity, inclusion radius, and liquid saturation. The numerical results demonstrate a significant dependence of energy shares of distinct reflected waves on the incident direction, saturation, porosity, inclusion radius, wave frequency, and WIFF.. The findings of this study fill a critical gap in understanding how these factors influence the propagation of seismic waves in unsaturated porous media, which is essential for reservoir interpretation, physical property inversion, and sediment type classification.

Field equations and constitutive relations

Following Shi et al.[44], the equations of motion in the absence of body force for each particle in an unsaturated porous solid are as follows:

$$\sigma^{(0)}_{ij,j} = \rho_{11}\ddot{u}_i + \rho_{12}\ddot{U}^{(1)}_i + \rho_{13}\ddot{U}^{(2)}_i - (m_1 - m_{12})(\dot{U}^{(1)}_i - \dot{u}_i) - (m_2 - m_{12})(\dot{U}^{(2)}_i - \dot{u}_i), \tag{1}$$

$$\sigma^{(1)}_{,i} = \rho_{12}\ddot{u}_i + \rho_{22}\ddot{U}^{(1)}_i + \rho_{23}\ddot{U}^{(2)}_i + m_1(\dot{U}^{(1)}_i - \dot{u}_i) - m_{12}(\dot{U}^{(2)}_i - \dot{u}_i), \tag{2}$$

$$\sigma^{(2)}_{,i} = \rho_{13}\ddot{u}_i + \rho_{23}\ddot{U}^{(1)}_i + \rho_{33}\ddot{U}^{(2)}_i - m_{12}(\dot{U}^{(1)}_i - \dot{u}_i) + m_2(\dot{U}^{(2)}_i - \dot{u}_i), \tag{3}$$

where the superscripts 0, 1, and 2 denote the porous solid's three phases: solid matrix, liquid, and gas. The indices are limited to the values 1, 2, and 3. Repeating an index signifies the involvement of a summation.The inclusion of a dot in the middle of a variable indicates partial differentiation in respect to time, while the inclusion of a comma in the head of an index signifies partial differentiation regarding space. The expressions of various elastic constants are described as

$$
\begin{aligned}
\rho_{11} &= \rho - 2(\rho_{f1}S_1 + \rho_{f2}S_2)\phi + (g_{12} + g_{13} + 2g_{23})\phi^2,\\
\rho_{12} &= \phi(\rho_{f1}S_1 - g_{12}\phi - g_{23}\phi),\\
\rho_{13} &= \phi(\rho_{f2}S_2 - g_{13}\phi - g_{23}\phi),\\
\rho_{22} &= g_{12}\phi^2,\\
\rho_{23} &= g_{23}\phi^2,\\
\rho_{33} &= g_{13}\phi^2,\\
\rho &= (1-\phi)\rho_s + \phi S_1\rho_{f1} + \phi S_2\rho_{f2},\\
g_{12} &= S_1\rho_{f1}F_s/\phi,\\
g_{13} &= S_2\rho_{f2}F_s/\phi,\\
g_{23} &= 0.1\sqrt{g_{12}g_{13}},\\
F_s &= ((1/\phi)+1)/2,\\
m_1 &= \tilde{b}_1\phi^2,\\
m_2 &= \tilde{b}_2\phi^2,\\
m_{12} &= \tilde{b}_{12}\phi^2,\\
k_{r1} &= \frac{(S_1-R_1)^2}{(1-R_1)^2},\\
k_{r2} &= \frac{(S_2-R_2)^2}{(1-R_2)^2},\\
k_{r12} &= \sqrt{0.1k_{r1}k_{r2}},\\
\tilde{b}_1 &= S_1^2\eta_{f1}/(\kappa k_{r1}),\\
\tilde{b}_2 &= S_2^2\eta_{f2}/(\kappa k_{r2}),\\
\tilde{b}_{12} &= S_1S_2k_{r12}\sqrt{\eta_{f1}\eta_{f2}}/D,\\
D &= \kappa(k_{r1}k_{r2} - k_{r12}^2)
\end{aligned}
$$

, $S_1 + S_2 = 1, \phi = \phi_1 + \phi_2 = \phi_{10}S_1 + \phi_{20}S_2$.

The constitutive relations (Shi et al.[44]) incorporating global flow and mesoscopic flow in the distinct phases of the porous medium are described in the following form:

$$\sigma_{ij}^{(0)} = \left[a_{11}u_{k,k} + a_{12}U_{k,k}^{(1)} + a_{13}U_{k,k}^{(2)}\right]\delta_{ij} + N(u_{i,j} + u_{j,i}), \tag{4}$$

$$\sigma^{(1)} = \left[a_{12}u_{k,k} + a_{22}U_{k,k}^{(1)} + a_{23}U_{k,k}^{(2)}\right]\delta_{ij}, \tag{5}$$

$$\sigma^{(2)} = \left[a_{13}u_{k,k} + a_{23}U_{k,k}^{(1)} + a_{33}U_{k,k}^{(2)}\right]\delta_{ij}, \tag{6}$$

$$\zeta = \gamma_1 u_{k,k} + \gamma_2 U_{k,k}^{(1)} + \gamma_3 U_{k,k}^{(2)}, \tag{7}$$

where ζ specifies the multiscale WIFF in unsaturated porous solid. The coefficients expressed in the aforementioned equations are delineated as

$$
\begin{aligned}
a_{11} =& A + \gamma_1\gamma_1/\gamma_0,\\
a_{12} =& Q_1 + \gamma_1\gamma_2/\gamma_0,\\
a_{13} =& Q_2 + \gamma_1\gamma_3/\gamma_0,\\
a_{22} =& R_1 + \gamma_2\gamma_2/\gamma_0,\\
a_{23} =& R_3 + \gamma_2\gamma_3/\gamma_0,\\
a_{33} =& R_2 + \gamma_3\gamma_3/\gamma_0,\\
A =& \lambda_c - 2B_1\phi - 2B_2\phi + (M_1 + M_2 + 2M_3)\phi^2,\\
\lambda_c =& K_c - (2N_m/3),\\
R_1 =& M_1\phi^2,\\
R_2 =& M_2\phi^2,\\
R_3 =& M_3\phi^2,\\
Q_1 =& \phi(B_1 - M_1\phi - M_3\phi),\\
Q_2 =& \phi(B_2 - M_2\phi - M_3\phi),\\
B_1 =& ((S_1 + \beta)\gamma - \beta + (\gamma - 1)\eta)\vartheta K_c,\\
B_2 =& (S_2 + (1 - \gamma)\eta)\vartheta K_c,\\
r =& (S_1 + \beta)/K_s + (qB_2 + (S_1 + \beta)(1 - (K_c/K_s)))/(K_c - K_m),\\
M_1 =& -\left(B_1/\delta K_m + M_3\right),\\
M_2 =& (B_2 r + \eta)/q,\\
M_3 =& -(1/K_m\delta + r/q)B_2 - \eta/q,\\
\delta =& \frac{1}{K_s} - \frac{1}{K_m},\\
\phi_{10} =& \phi_{20} = \phi,\\
\phi_1 =& \phi S_1,\\
\phi_2 =& \phi S_2,\\
q =& \phi((1/K_{f1}) + (1/P'_{ca}S_1S_2)),\\
\gamma =& (1 + P'_{ca}S_1S_2/K_{f2})/(1 + P'_{ca}S_1S_2/K_{f1}),\\
\alpha' =& 1 + (\gamma - 1)(S_1 + \beta),\\
K_f =& \alpha'((\gamma S_1/K_{f1}) + (S_2/K_{f2}))^{-1},\\
G =& (K_m - K_s)K_f/(\phi(K_f - K_s)),\\
K_c =& (K_m + G)K_s/(K_s + G),\\
\vartheta =& ((1/K_s) - (1/K_m) + \phi((1/K_m) - (1/K_c)))/(\alpha'((1/K_s) - (1/K_m) + \phi((1/K_m) - (1/K_f)))),\\
P_{ca} =& A[(S_1 + S_{r2} - 1)^{-2} - ((S_{r1}/S_1)^2)(1 - S_{r1} - S_{r2})^{-2}),\\
P'_{ca} =& \frac{dP_{cp}}{dS_1},\\
\beta =& P_{ca}/P'_{ca}, \eta = P_w/P'_{ca},\\
\gamma_0 =& -((1/3)R_0^2\phi_1^2\phi_2\phi_{20}((\rho_{f1}\omega^2/\phi_{10}) + (\iota\omega\eta_{f1}/\kappa)) + R_1\phi_2^2 + R_2\phi_1^2 - 2R_3\phi_1\phi_2),\\
\gamma_1 =& (Q_1\phi_2 - Q_2\phi_1),\\
\gamma_2 =& (R_1\phi_2 - R_3\phi_1),\\
\gamma_3 =& (R_3\phi_2 - R_2\phi_1).
\end{aligned}
$$

Utilising constitutive relations inside the equations of motion, we formulate the equations of motion by means of the displacement components. The equations are expressed as follows:

$$
\begin{aligned}
(a_{11} + N)u_{j,ij} + a_{12}U^{(1)}_{j,ij} + a_{13}U^{(2)}_{j,ij} + Nu_{j,ij} =& \rho_{11}\ddot{u}_i + \rho_{12}\ddot{U}^{(1)}_i + \rho_{13}\ddot{U}^{(2)}_i\\
& -(m_1 - m_{12})(\dot{U}^{(1)}_i - \dot{u}_i)(m_2 - m_{12})(\dot{U}^{(2)}_i - \dot{u}_i),\\
a_{12}u_{j,ij} + a_{22}U^{(1)}_{j,ij} + a_{23}U^{(2)}_{j,ij} =& \rho_{12}\ddot{u}_i + \rho_{22}\ddot{U}^{(1)}_i + \rho_{23}\ddot{U}^{(2)}_i\\
& +m_1(\dot{U}^{(1)}_i - \dot{u}_i) - m_{12}(\dot{U}^{(2)}_i - \dot{u}_i),\\
a_{13}u_{j,ij} + a_{23}U^{(1)}_{j,ij} + a_{33}U^{(2)}_{j,ij} =& \rho_{13}\ddot{u}_i + \rho_{23}\ddot{U}^{(1)}_i + \rho_{33}\ddot{U}^{(2)}_i\\
& -m_{12}(\dot{U}^{(1)}_i - \dot{u}_i) + m_2(\dot{U}^{(2)}_i - \dot{u}_i).
\end{aligned}
\tag{8}
$$

Plane harmonic wave propagation

To examine the propagation properties of planar harmonic waves in the specified medium, we postulate the assumption

$$\left\{u_j, U_j^{(1)}, U_j^{(2)}\right\} = \left\{\bar{S}_j, \bar{L}_j, \bar{G}_j\right\} e^{\{\iota\omega(p_k x_k - t)\}}, \tag{9}$$

where the slowness vector is denoted by the expression (p_1, p_2, p_3) and the angular frequency is depicted by the symbol ω. When the phase velocity V is considered, the concept of slowness may be described as $(p_1, p_2, p_3) = \mathbf{N}/V$. It is possible to use the row matrix $\mathbf{N} = (n_1, n_2, n_3)$ to represent the direction of phase propagation. The vectors $(\bar{S}_1, \bar{S}_2, \bar{S}_3)$, $(\bar{L}_1, \bar{L}_2, \bar{L}_3)$, and $(\bar{G}_1, \bar{G}_2, \bar{G}_3)$, respectively, constitute the representations of the polarisations of the solid and fluid particles that are present in the composite medium. By inserting (9) into the equation (8), we have a set of equations, which are as follows:

$$\left[(a_{11} + N)n_i n_j + (N - b_{11}V^2)\delta_{ij}\right]\bar{S}_j + \left[a_{12}n_i n_j - b_{12}V^2\delta_{ij}\right]\bar{L}_j + \left[a_{13}n_i n_j - b_{13}V^2\delta_{ij}\right]\bar{G}_j = 0, \tag{10}$$

$$\left[a_{12}n_i n_j - b_{12}V^2\delta_{ij}\right]\bar{S}_j + \left[a_{22}n_i n_j - b_{22}V^2\delta_{ij}\right]\bar{L}_j + \left[a_{23}n_i n_j - b_{23}V^2\delta_{ij}\right]\bar{G}_j = 0, \tag{11}$$

$$\left[a_{13}n_i n_j - b_{13}V^2\delta_{ij}\right]\bar{S}_j + \left[a_{23}n_i n_j - b_{23}V^2\delta_{ij}\right]\bar{L}_j + \left[a_{33}n_i n_j - b_{33}V^2\delta_{ij}\right]\bar{G}_j = 0, \tag{12}$$

where

$$b_{11} = \rho_{11} + \frac{\iota}{\omega}(m_1 + m_2 - 2m_{12}), \quad b_{12} = \rho_{12} - \frac{\iota}{\omega}(m_1 - m_{12}), \quad b_{13} = \rho_{13} - \frac{\iota}{\omega}(m_2 - m_{12}),$$
$$b_{22} = \rho_{22} + \frac{\iota}{\omega}m_1, \quad b_{23} = \rho_{23} - \frac{\iota}{\omega}m_{12}, \quad b_{33} = \rho_{33} + \frac{\iota}{\omega}m_2.$$

In order to establish a connection between the three types of displacements, namely $\mathbf{u}$, $\mathbf{U}^{(1)}$, and $\mathbf{U}^{(2)}$, the Eqs. (10), (11) and (12) are solved as follows.

$$\bar{L}_i = \Gamma_{ij}\bar{S}_j; \qquad \Gamma = \frac{b_0}{a_0}\left(\mathbf{I} - \mathbf{N}^T\mathbf{N}\right) + \frac{b_0V^4 + b_1V^2 + b_2}{a_0V^4 + a_1V^2 + a_2}\mathbf{N}^T\mathbf{N}, \tag{13}$$

$$\bar{G}_i = \Delta_{ij}\bar{S}_j; \qquad \Delta = \frac{c_0}{a_0}\left(\mathbf{I} - \mathbf{N}^T\mathbf{N}\right) + \frac{c_0V^4 + c_1V^2 + c_2}{a_0V^4 + a_1V^2 + a_2}\mathbf{N}^T\mathbf{N}. \tag{14}$$

In this context, the depiction $\mathbf{N}^T$ signifies the transpose of the row matrix $\mathbf{N}$, whereas the description $\mathbf{I}$ is a three-dimensional identity matrix. The aforementioned equations establish a number of constants, and the different constants are provided by

$$a_0 = b_{22}b_{33} - b_{23}^2, a_1 = 2a_{23}b_{23} - a_{22}b_{33} - a_{33}b_{22}, a_2 = a_{22}a_{33} - a_{23}^2,$$
$$b_0 = b_{23}b_{13} - b_{12}b_{33}, b_1 = a_{12}b_{33} + a_{33}b_{12} - a_{13}b_{23} - a_{23}b_{13}, b_2 = a_{13}a_{23} - a_{12}a_{33},$$
$$c_0 = b_{12}b_{23} - b_{13}b_{22}, c_1 = a_{13}b_{22} + a_{22}b_{13} - a_{12}b_{23} - a_{23}b_{12}, c_2 = a_{12}a_{23} - a_{13}a_{22}.$$

When we put equations (13) and (14) into equation (10), we get a set of three equations, which are as follows:

$$\left[a_3\mathbf{N}^T\mathbf{N} + b_3\left(\mathbf{I} - \mathbf{N}^T\mathbf{N}\right)\right]\bar{\mathbf{S}} = 0, \tag{15}$$

which are the Christoffel equations that describe the propagation of harmonic plane waves in a porous material. Following is a description of the coefficients that are utilised in a number of relations are as follows:

$$a_3 = \left(a_{11} + 2N - b_{11}V^2\right)\left[a_0V^4 + a_1V^2 + a_2\right] + (a_{12} - b_{12}V^2)[b_0V^4 + b_1V^2 + b_2]$$
$$+ (a_{13} - b_{13}V^2)[c_0V^4 + c_1V^2 + c_2],$$
$$b_3 = N - \left[b_{11} + b_{12}\frac{b_0}{a_0} + b_{13}\frac{c_0}{a_0}\right]V^2.$$

It is possible to determine the determinant of the coefficient matrix, which is provided by $a_3\mathbf{N}^T\mathbf{N} + b_3(\mathbf{I} - \mathbf{N}^T\mathbf{N})$. This determinant may be expressed as $(b_3a_3^2)$. It is essential that the determinant $(b_3a_3^2)$ be equal to zero in order to ensure that the Christoffel equations (15) need a solution that is not trivial. In the case whenever the value of a_3 is equal to zero, we are able to deduce the following mathematical relationship:

$$d_3V^6 + d_2V^4 + d_1V^2 + d_0 = 0, \tag{16}$$

where

$$d_3 = b_{11}a_0 + b_{12}b_0 + b_{13}c_0,$$
$$d_2 = b_{11}a_1 + b_{12}b_1 + b_{13}c_1 - (a_{11} + 2N)a_0 - a_{12}b_0 - a_{13}c_0,$$
$$d_1 = b_{11}a_2 + b_{12}b_2 + b_{13}c_2 - (a_{11} + 2N)a_1 - a_{12}b_1 - a_{13}c_1,$$
$$d_0 = -(a_{11} + 2N)a_2 - a_{12}b_2 - a_{13}c_2.$$

In this particular circumstance, the polarisations $\bar{\mathrm{S}}$ align themselves in a manner that is complementary to the phase direction $\mathbf{N}$. This demonstrates that the equation presented before has accurately described the propagation of dilatational waves. An unsaturated porous medium is characterised by the presence of three dilatational waves, and the propagation of these waves is characterised by three roots of the cubic equation (16) in terms of V^2. Because of the existence of viscous pore fluids, a medium is believed to be dissipative. In light of this, equation (16) has complex roots, which suggests that dilatational waves in the medium are subject to attenuation. The four dilatational waves with velocity order $\Re(V_1) > \Re(V_2) > \Re(V_3)$ are referred to as $P_1,\ P_2,\ P_3$ waves, respectively, for the purpose of making the discussion more convenient.

Another equation, namely $b_3 = 0$, produces

$$V = \sqrt{N/\left[b_{11} + b_{12}\frac{b_0}{a_0} + b_{13}\frac{c_0}{a_0}\right]}. \tag{17}$$

n this scenario, the polarisation $\bar{\mathrm{S}}$ is orientated perpendicular to the propagation direction $\mathbf{N}$. This equation will define the velocity of a transverse wave in a medium that sustains attenuation as a result of the viscosity of the fluid contained beneath its pores. The solitary transverse wave is considered to be the SV wave.

Reflection at plane boundary

The purpose of the investigation is to explore the consequences of porosity, water saturation, wave frequency, and inclusion radius on the fluid flow and energy distribution of reflected waves at the stress-free surface of a unsaturated porous material.

Definition of the problem

Consider a rectangular coordinate system (x, y, z), where the region $z > 0$ consists of a porous medium saturated with two immiscible viscous fluids that permeate farther in the z-direction. The plane described by the equation $z = 0$ is regarded as the stress-free surface of this material (Fig. 1). The substantial attenuation of a seismic wave may be more explicitly shown by its irregular propagation. Thus, the extensive propagation of an attenuated wave in a dissipative medium is regarded as inhomogeneous. This is determined by the alignment of the propagation vector and the divergence of the attenuation vector from the propagation vector. Consequently, two angles, namely θ_0 and γ_0, are necessary to describe an inhomogeneous incident wave (Fig. 1). As stated by Borcherdt[45], horizontal slowness may be determined through θ_0 (angle of propagation), γ_0 (angle of attenuation), A (attenuation vector), and P (propagation vector).

$$s = |\mathrm{P}|\sin\theta_0 - \iota|\mathrm{A}|\sin(\theta_0 - \gamma_0). \tag{18}$$

Consequently, for an incident wave with velocity V_0, we have

$$|\mathrm{P}|^2 = \frac{1}{2}[\Re(\frac{\omega^2}{V_0^2}) + \sqrt{(\Re(\frac{\omega^2}{V_0^2}))^2 + (\Im(\frac{\omega^2}{V_0^2}))^2/\cos^2\gamma_0}], \tag{19}$$

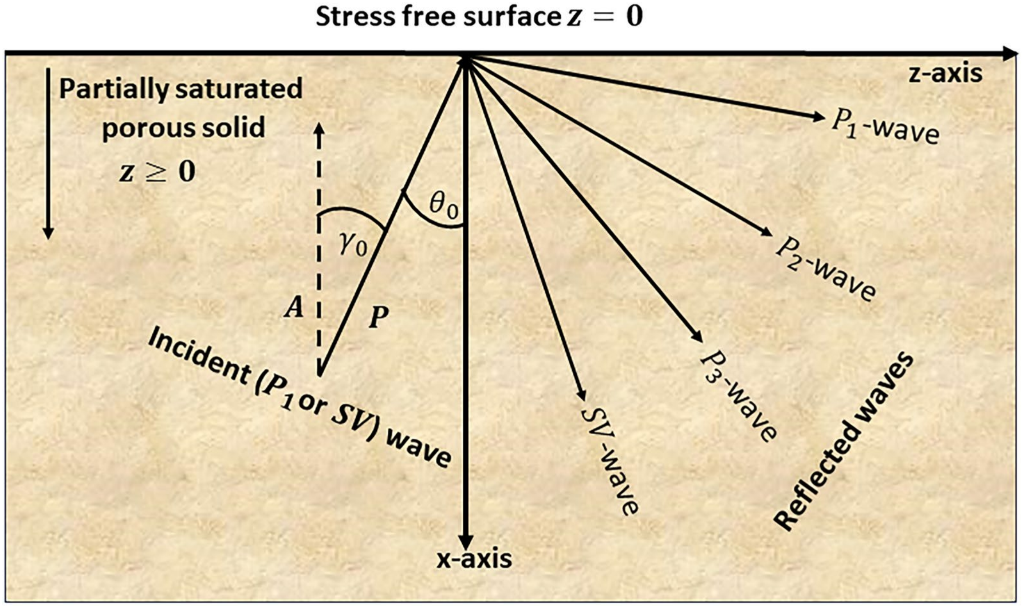

Fig. 1. Schematic diagram of the problem.

$$|\mathrm{A}|^2 = \frac{1}{2}[-\Re(\frac{\omega^2}{V_0^2}) + \sqrt{(\Re(\frac{\omega^2}{V_0^2}))^2 + (\Im(\frac{\omega^2}{V_0^2}))^2/\cos^2\gamma_0}]. \tag{20}$$

The dissipative characteristics of the porous medium need the specification of the incident wave at the boundary $z = 0$ about its propagation direction (θ_0) and attenuation direction (γ_0). The vector $(s, 0, q_0)$ depicts the slowness vector of the incident wave, with $q_0(= \pm\sqrt{1/V_0^2 - s^2})$ indicating the vertical slowness of the incident wave. For the incident wave to propagate towards the boundary in the negative z-direction, the real part of q_0 must be negative. Snell's law stipulates that the horizontal slowness (s) of both incident and reflected waves is invariant. The vector $(s, 0, q_k)$ depicts the slowness vector for reflected waves, where $q_k = \pm\sqrt{1/V_k^2 - s^2}, (k = 1, 2, 3, 4)$. To ensure the dissipation of reflected waves travelling away from the boundary in the positive z-direction, the imaginary part of q_k must be greater than zero.

In the subsequent step, the aggregate displacement of material particles in the medium is equal to the combination of the displacements corresponding to the wave that strikes the medium and the four waves that reflect off of it. Consequently, the depiction of the overall displacement of material particles in the $xz-$plane for two dimensions motion may be represented as follows:

$$\begin{aligned} u_j =& [\bar{S}_j^{(0)} \exp(-\iota\omega q_0 z) + \sum_{k=1}^{4} \epsilon_k \bar{S}_j^{(k)} \exp\{\iota\omega(sx + q_k z - t)\}], \\ U_j^{(1)} =& [\bar{L}_j^{(0)} \exp(-\iota\omega q_0 z) + \sum_{k=1}^{4} \epsilon_k \bar{L}_j^{(k)} \exp\{\iota\omega(sx + q_k z - t)\}], \\ U_j^{(2)} =& [\bar{G}_j^{(0)} \exp(-\iota\omega q_0 z) + \sum_{k=1}^{4} \epsilon_k \bar{G}_j^{(k)} \exp\{\iota\omega(sx + q_k z - t)\}], \quad (j = x, z), \end{aligned} \tag{21}$$

The excitation factors for reflected waves are denoted by the ϵ_k symbol. These factors are related to the incident wave. The index '0' is used to signify the wave that is incident. In this context, the index 'k'$(= 1, 2, 3, 4)$ is used to denote the reflected waves (P_1, P_2, P_3, SV) simultaneously. There is a possibility of defining the polarisation of a longitudinal and transverse waves by using the unit vector n, which may be computed as $\mathrm{n} = (s, 0, q_k)V_k$.

Boundary conditions

The current geometry incorporates boundary constraints for particle motion at the stress-free planar surface at $z = 0$. This study considers impermeable boundary conditions, namely sealed holes, at the plane defined by $z = 0$. At an impermeable barrier consisting of sealed pores, there is no flow of interstitial fluid permitted at the surface when waves pass through the plane at $z = 0$. Therefore, the appropriate boundary conditions that must be fulfilled at the plane $z = 0$ are as follows:

$$\begin{aligned} i)\ \sigma_{zz}^{(0)} =& 0, \\ ii)\ \sigma_{zx}^{(0)} =& 0, \\ iii)\ U_z^{(1)} =& 0, \\ iv)\ U_z^{(2)} =& 0. \end{aligned} \tag{22}$$

Reflection coefficients

To formulate an array of four contemporaneous non-homogeneous linear equations, we must first resolve the four boundary conditions (22) using the displacement articulated in Eq. (21). The following expressions represent the system of four equations:

$$\sum_{k=1}^{4} f_{lk}\epsilon_k = -f_{l0}, \qquad (l = 1, 2, 3, 4). \tag{23}$$

For $(k = 1, 2, 3, 4)$, we have

$$\begin{aligned} f_{1k} =& a_{11}[s\bar{S}_x^{(k)} + q_k\bar{S}_z^{(k)}] + a_{12}[s\bar{L}_x^{(k)} + q_k\bar{L}_z^{(k)}] + a_{13}[s\bar{G}_x^{(k)} + q_k\bar{G}_z^{(k)}] + 2Nq_kS_z^{(k)}, \\ f_{2k} =& N[q_k\bar{S}_x^{(k)} + s\bar{S}_z^{(k)}], \quad f_{3k} = \bar{L}_z^{(k)}, \quad f_{4k} = \bar{G}_z^{(k)}. \end{aligned}$$

The system of equations, represented by the variables ϵ_k (where $k = 1,\ 2,\ 3,\ 4$), is solved employing the Gauss elimination technique. These unknown entities might be referred to as reflection coefficients.

Wave-induced fluid flow

With the aid of the relations (13) and (14) in equation (7), the WIFF in pores can only be discovered as a result of the dilation of solid particles, and it is described as follows:

$$\zeta = [\lambda_1 + \lambda_2\Gamma(V) + \lambda_3\Delta(V)](u_{x,x} + u_{z,z}). \tag{24}$$

By applying equation (21) to the equation that came before it, we could derive

$$\zeta(V_k) = \iota\omega\epsilon_k[\lambda_1 + \lambda_2\Gamma(V_k) + \lambda_3\Delta(V_k)](sA_x^k + q_k A_z^k)e^{\iota\omega(sx+q_k z-t)}, (k = 1, 2, 3, 4). \tag{25}$$

We can verify that $\zeta(V_4) = 0$ by integrating the shear wave existence condition into the equation as mentioned above. It suggests that three longitudinal waves regulate the movement of WIFF inside pores. Hence, the functions $\varsigma(V_1), \zeta(V_2), \varsigma(V_3)$ represent the individual contribution of P_1, P_2, P_3 to the overall fluid flow. Since V_k is a complex number, it follows that $\varsigma(V_k)$ is also a complex number. The fluid flow caused by longitudinal waves, denoted as ζ_k, is a physical quantity that may be determined as the real component of its complex form, which is represented as $\zeta_k = \Re(\zeta(V_k))$. The sum of ζ_1, ζ_2, and ζ_3 represents the overall fluid flow that occurs in a partly saturated porous solid when a P_1 (or *SV*) wave is placed to the stress-free surface of a partially saturated porous solid comprising two viscous fluids (immiscible).

Energy partition

This article seeks to analyse the partitioning of energy from incident wave into distinct reflected waves. The energy transferred per unit area in the plane $z = 0$ is determined by computing the scalar product of the surface traction and particle velocity as outlined by Achenbach[46]. The existence of a dissipative porous medium results in energy dissipation, necessitating the consideration of interaction energy (Borcherdt[45]; Krebes[47]) or interference energy (Ainslie and Burns[48]) between two waves with distinct characteristics. Consequently, the total energy flow comprises the energy flux transmitted by reflected waves and the interaction energy between two distinct types of waves. The medium now enables the transmission of five waves: one incident and four reflected. Consequently, an energy matrix is formulated to delineate the distribution of incoming energy at the surface $z = 0$.

$$E_{lk} = \Re(P_{lk}\epsilon_l\bar{\epsilon_k})/\Re(P_{55}), \qquad (l, k = 1, 2, 3, 4, 5); \tag{26}$$

where $\epsilon_5 = 1$. A bar above a complex number signifies its conjugate. The components P_{lk} in Eq. (26) are defined by

$$\begin{aligned} P_{lk} = &\left[a_{11}[s\bar{S}_x^{(l)} + q_l\bar{S}_z^{(l)}] + a_{12}[s\bar{L}_x^{(l)} + q_l\bar{L}_z^{(l)}] + a_{13}[s\bar{G}_x^{(l)} + q_l\bar{G}_z^{(l)}] + 2Nq_lS_z^{(l)}\right]\bar{S}_z^{(k)} \\ &+G\left[s\bar{S}_z^{(l)} + q_l\bar{S}_x^{(l)}\right]\bar{\bar{S}}_x^{(k)} + X_l\bar{\bar{L}}_z^{(k)} + Y_l\bar{\bar{G}}_z^{(k)}, \end{aligned} \tag{27}$$

where

$$\begin{aligned} X_l &= a_{12}[s\bar{S}_x^{(i)} + q_k\bar{S}_z^{(l)}] + a_{22}[s\bar{L}_x^{(l)} + q_k\bar{L}_z^{(l)}] + a_{23}[s\bar{G}_x^{(l)} + q_k\bar{G}_z^{(l)}] \\ Y_l &= a_{13}[s\bar{S}_x^{(i)} + q_k\bar{S}_z^{(l)}] + a_{23}[s\bar{L}_x^{(l)} + q_k\bar{L}_z^{(l)}] + a_{33}[s\bar{G}_x^{(l)} + q_k\bar{G}_z^{(l)}]. \end{aligned}$$

When dealing with porous media, the energy matrix E_{ij}, $(i, j = 1,\ 2,\ 3,\ 4,\ 5)$ is used to ascertain the energy proportions of four reflected waves, which are represented by the symbols P_1, P_2, P_3, and *SV* accordingly. It is possible to differentiate the energy proportions of the reflected waves P_1, P_2, P_3, and *SV* by referring to the diagonal entries E_{11}, E_{22}, E_{33}, and E_{44}. In order to determine the interaction energy that results from the interference of the incident wave with each reflected wave, the equation $E_{IR} = \sum_{i=1}^{4}(E_{5i} + E_{i5})$ becomes applicable. It is possible to determine the interaction energy between every pair of reflected waves by using the expression $E_{RR} = \sum_{i=1}^{4}(\sum_{j=1}^{4} E_{ij} - E_{ii})$. It is necessary for the aggregate bulk energies of the reflected waves and the overall interaction energy to be equal to the bulk energy of the incident wave at the stress-free surface to satisfy the law of energy conservation requirements.

$$\sum_{i=1}^{4} E_{ii} + E_{RR} + E_{IR} = -E_{55} = 1. \tag{28}$$

During the whole process of reflection, it is essential that the energy balance law at the stress-free surface be maintained at each and every angle of incidence. This law is known as the energy balance law. As a consequence, relation (28) guarantees the preservation of energy at the surface that is free of stress.

Numerical example

We employ a numerical model of an unsaturated porous solid to examine the impact of wave frequency, incidence direction, and elastic properties like porosity, inclusion radius, and liquid saturation on reflection characteristics and WIFF. A reservoir rock (sandstone) saturated with water and CO_2 is chosen for the numerical model of porous medium. Table 1 contains information on the sandstone's elastic and dynamic constants.

Parameter (unit)	Value	Parameter (unit)	Value
K_s (GPa)	12	K_m (GPa)	6.21
N_m (GPa)	9.55	κ (Darcy)	1
ρ_s (kg/m^3)	2650	ϕ	0.33
ρ_{f1} (kg/m^3)	1000	ρ_{f2} (kg/m^3)	100
η_{f1} (Pa.s)	0.001	η_{f2} (Pa.s)	0.00015
K_{f1} (GPa)	2.223	K_{f2} (GPa)	0.022
S_{r1}	0.05	S_{r2}	0.05
A	3000	P_w (MPa)	45

Table 1. The parameters of sandstone that has been saturated with gas and water.

Numerical discussion
Partitioning of incident energy among reflected waves
P_1-wave incidence

Figure 2 illustrates how porosity affects the distribution of energy in reflected waves at the stress-free surface of closed pores. It has been seen that the energy share of the P_1 waves is increasing as the porosity (ϕ) increases. The phenomenon is also seen in all other refracted waves, however these waves experience a decrease in energy distribution as porosity increases. The energy partitions clearly indicate that the bulk of the energy is distributed between the P_1 and *SV* waves. The P_1 wave energy decreases as the angle rises from normal incidence. Following a minimum at around 40^0, the energy progressively rises until it reaches grazing incidence. The reflected *SV* wave exhibits contrasting behavior, indicating the conversion of energy at the surface. The graphs of bulk energy shares for various reflected waves exhibit that at normal and grazing incidence, only the reflected P_1 wave remains. In contrast, the *SV* wave does not survive at any angle [Yang and Sato[49]]. The energy proportions of reflected P_2 and P_3 waves are minimal. This is attributable to the fact that the phase speeds of these waves are much lower than those of all other wave modes. The energy shares of slower waves diminish as the angle of incidence rises. The calculations have been validated against the principle of energy conservation. The graphs of bulk energy shares for various reflected waves clearly indicate that energy conservation is observed at every angle of incidence. This proves the validity of the energy balance law as articulated in Eq. (25). It confirms that the numerical computations are analytically accurate.

Figure 3 illustrates the effect of wave frequency on the allocation of incident energy among four reflected waves in a partly saturated porous medium. The image displays that the P_1 wave first intensifies with increasing frequency. However, the influence of frequency becomes negligible upon attaining an angle of $\theta_0 = 45°$. The increasing ω amplifies the energy contribution of the *SV* wave. The energy dispersion is more significant for slower waves, substantially diminishing the P_3 wave at low frequencies. Further, there is a substantial increase in the energy distribution of the P_2 wave with rising frequency. The correlation between energy shares and frequency may enhance fluid content prediction in seismic data interpretation and facilitate the development of novel processing techniques for evaluating fluid characteristics from seismic data.

The effect of water saturation, denoted by the symbol S_2, on the energy distributions of reflected waves is seen in Figure 4. Figure 3 illustrates that the energy shares at the stress-free surface of an unsaturated poroelastic material may go through considerable changes depending on its frequency. A change in the saturation of the fluid may bring about a substantial change in the frequency-dependent behaviour of the fluid, which in turn brings about a significant change in the energy shares associated with the fluctuations in water saturation. An increase in S_2 decreases the strength of the P_1 wave. On the contrary, the rest of the waves showed a substantial rise when S_2 grew. The faster waves exhibit an opposing behavior compared to the incidence direction (θ_0). The energy ratios of slower waves exhibit comparable fluctuations. The interference energy is notably enriched when the value of S_2 grows, mainly when the incidence is normal.

The radius of spherical inclusions embedded in a partially saturated porous media plays a significant role in determining the heterogeneity scale of the rock. Consequently, it has a direct impact on the way seismic waves propagate. Figure 5 demonstrates how altering the value of R_0 impacts the energy distribution among the four reflected plane waves. It is evident from this figure that the inclusion radius has a substantial impact on the reflection coefficients. As R_0 grows, the contrast in P_1 wave impedance increases, resulting from a more significant magnitude of the reflected P_1 wave. Consequently, the energy distribution of the reflected waves is altered correspondingly. The rise in R_0 greatly intensified the P_1 wave. However, when the value of R_0 grows, the *SV* wave becomes less prominent. In proportion to the rise in R_0, the energy shares of slower waves are decreasing.

The impacts of WIFF on the ways in which incident energy is distributed across four reflected waves are seen in Fig. 6. In the presence of WIFF, the P_1 wave is enhanced between the values of 0 and 25^0, while it is diminished between the values of θ_0 and 25^0. For values of 0 to 90^0, the existence of WIFF results in the enhancement of the P_2 and *SV* waves. The existence of WIFF, on the other hand, causes the P_3 wave to be weakened throughout the whole spectrum of incidence directions.

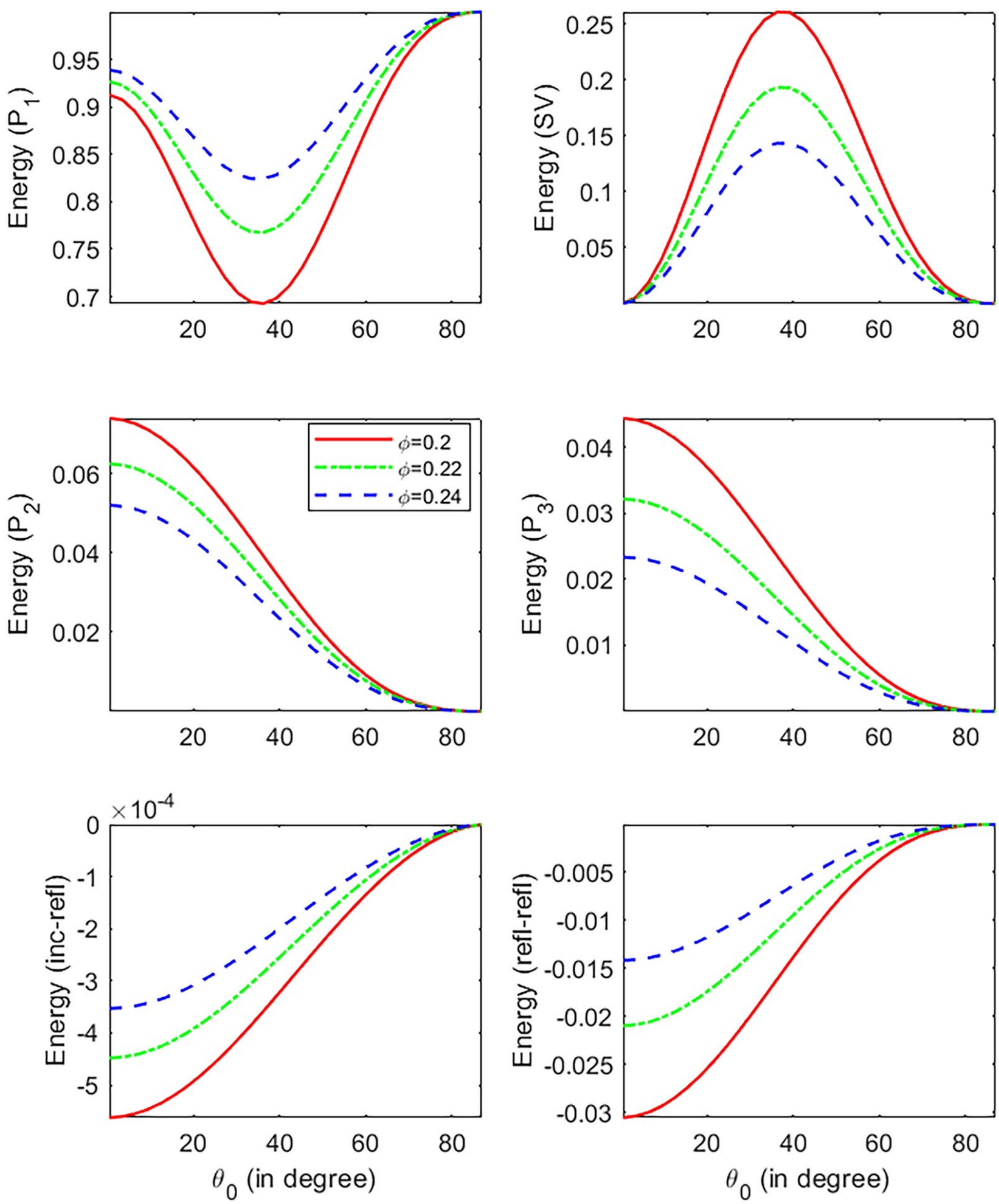

Fig. 2. Energy shares as a function of the incidence direction (θ_0) with different porosity (incident P_1 wave).

SV-wave incidence

To determine the incidence of a *SV* wave, we will analyze the distribution of incident energy among many reflected waves. The differences in the energy distribution of the reflected waves are shown in Fig. 7, which plots the variances as a function of frequency and incidence angles. On all of the waves, a reversal effect of porosity is noticed, which is in contrast to the wave with the incidence P_1 shown in Fig. 1. A critical angle is regularly seen during the reflection of elastic waves. When the angle of incidence is exceeded, the energy flow vector of the associated wave mode begins to propagate in a direction parallel to the contact. A critical angle of around 45° is found for the reflected P_1 wave. In the vicinity of 45°, the energy ratio of the reflected P_1 wave becomes unimportant. The P_1 wave undergoes degeneration and transforms into an interface wave, which does not convey vertical energy flow. Concerning other reflected waves outside the critical angle, the reflected *SV* wave is given precedence. The contribution of the P_1 wave to the total energy is reduced as the value of ϕ increases. The energy shares of slower waves show similar variations. The slower waves beyond the critical incidence become more significant as θ_0 increases. The influence of interference energy from the interaction between incoming and reflected waves on energy preservation is negligible at all angles of incidence. Nonetheless, energy conservation is substantially affected by the interference energy between reflected waves.There is a strong indication from the graphs of bulk energy shares for the different reflected waves that the only wave that survives at both normal and grazing incidence is the reflected *SV* wave, while the P_1 wave does not survive at either angle (Yang and Sato[49]).

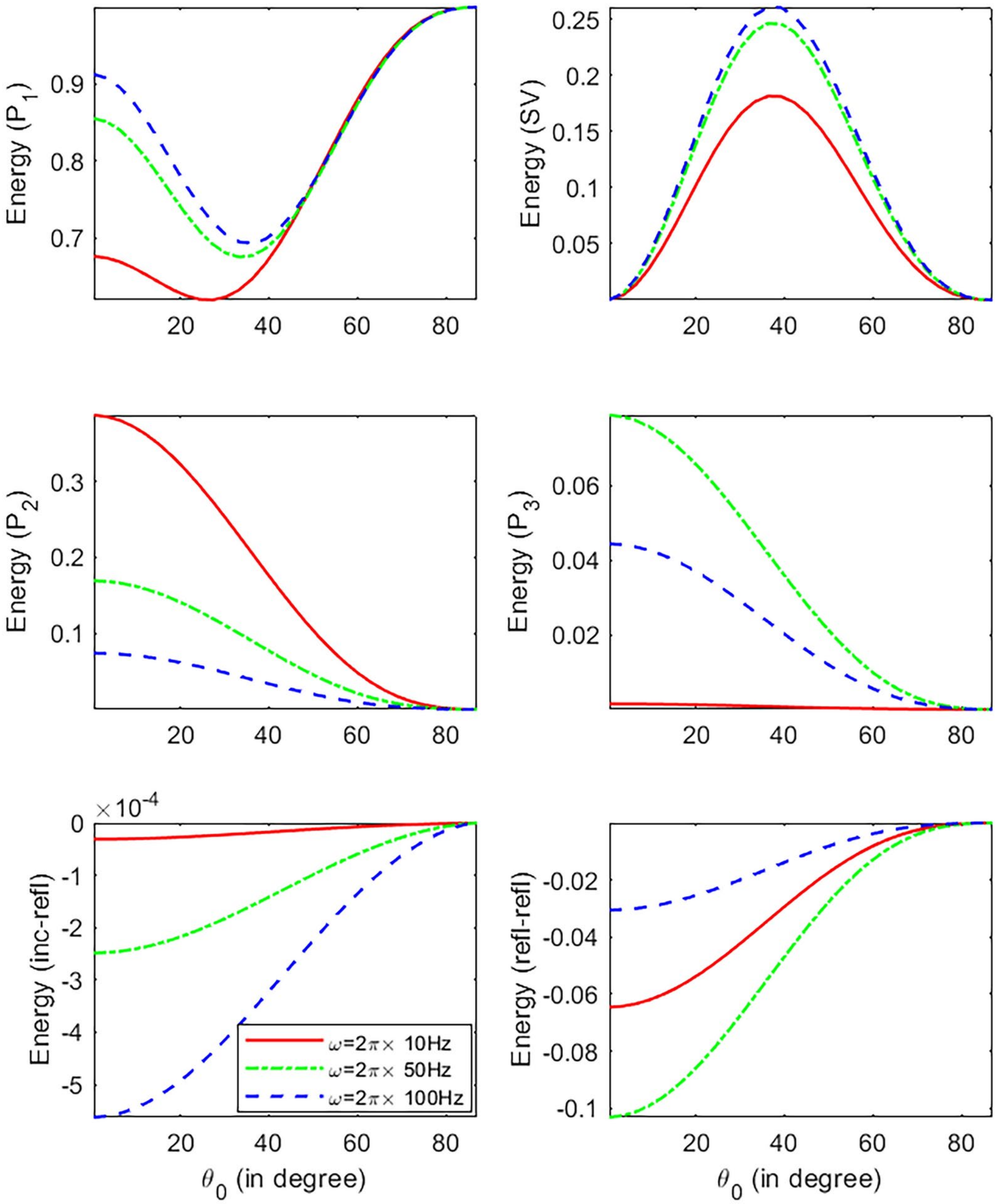

Fig. 3. Energy shares as a function of the incidence direction (θ_0) with different frequency (incident P_1 wave).

The influence of frequency on the distribution of incident energy among the four reflected waves is seen in Fig. 8. According to the data shown in this figure, the energy proportions of the P_1 wave grow as the frequency of the wave increases. In the same vein, the rising ω increases the energy share of the *SV* wave. Nevertheless, when θ_0 is less than or equal to 25^0, this increase loses its significance. The energy dispersion is more visible for slower waves, which leads to an extensive weakening of the P_3 wave at low frequencies. Furthermore, as the frequency rises, there is a discernible reduction in the proportion of energy that goes into the P_2 wave. As the angle of incidence, denoted by θ_0, grows, the significance of the contribution made by slower waves going beyond the critical incidence becomes more significant.

Figure 9 illustrates the effect of saturation on the energy distribution via incidence angles. Just as in the case of incident wave P_1 shown in Fig. 4, changes in water saturation have a substantial impact on the distribution of energy. The energy shares of longitudinal waves were significantly enhanced when S_2 increased. Furthermore, the slower P_2 wave experiences a significant rise in strength as water saturation increases, especially for $S_2 = 0.9$ beyond the critical incidence. On the contrary, the *SV* wave is weakened as S_2 increased.

Figure 10 illustrates the effect of changing the value of R_0 on the energy distribution among the four reflected plane waves. The graphic demonstrates that the inclusion radius significantly affects all the reflection coefficients. As R_0 increases, the proportion of energy attributed to longitudinal waves decreases. On the contrary, the *SV* wave diminished as the value of R_0 increased. Like the incident wave P_1 in Fig. 5, slower waves became stronger

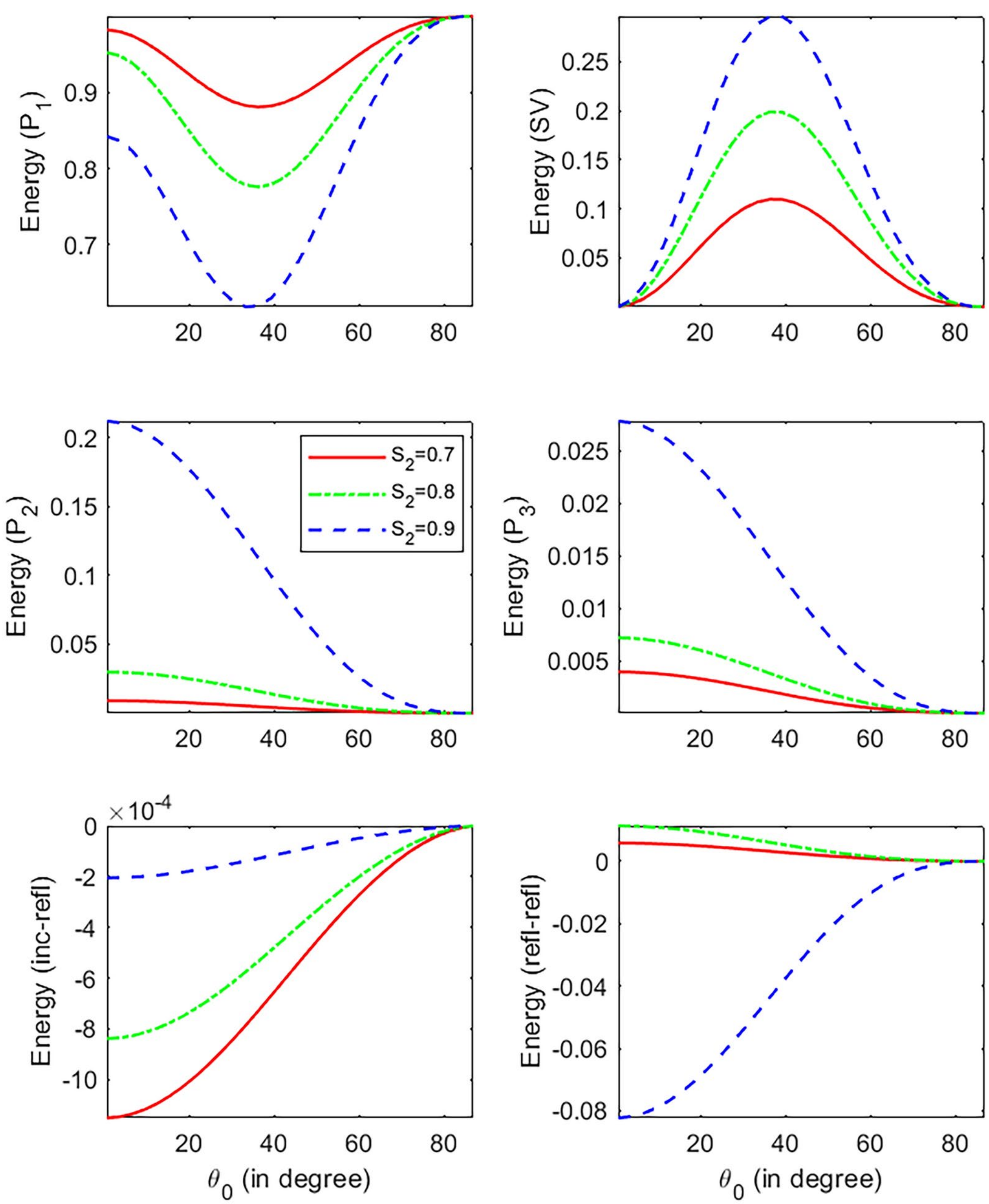

Fig. 4. Energy shares as a function of the incidence direction (θ_0) with different water saturation (incident P_1 wave).

as R_0 increased. However, the quicker waves are affected differently by the inclusion radius in comparison to the incident P_1 wave.

In Fig. 11, we illustrate the impact that WIFF has on the distribution of incident energy among four reflected waves. The P_1 wave is strengthened in the presence of WIFF below their critical incidence. The *SV* wave is weakened for $0 \leq \theta_0 \leq 55^0$ and strengthened for $\theta_0 > 35^0$ in the presence of WIFF. Figure 6 depicts similar behavior for P_2 and P_3 waves, and thus, it may be deduced that a similar impact of WIFF on P_2 and P_3 waves appeared for both incident waves (i.e., P_1 and *SV*).

Longitudinal waves contribution to WIFF

P_1-wave incidence

In this study, we investigate the function that longitudinal waves play in the flow of fluids at the stress-free surface of a partly saturated porous material. The investigation takes into account three distinct measures of porosity, denoted by (ϕ), water saturation, denoted by (S_2), and inclusion radius, denoted by (R_0), as seen in Figs. 12, 13 and 14. From these figures, it is possible to conclude that waves P_1 and P_2 are the primary contributors to fluid flow throughout the system. Since the porosity, water saturation, and inclusion radius are all increasing, the fluid flow caused by these waves may decrease. On the other hand, the contribution of wave P_2 diminishes

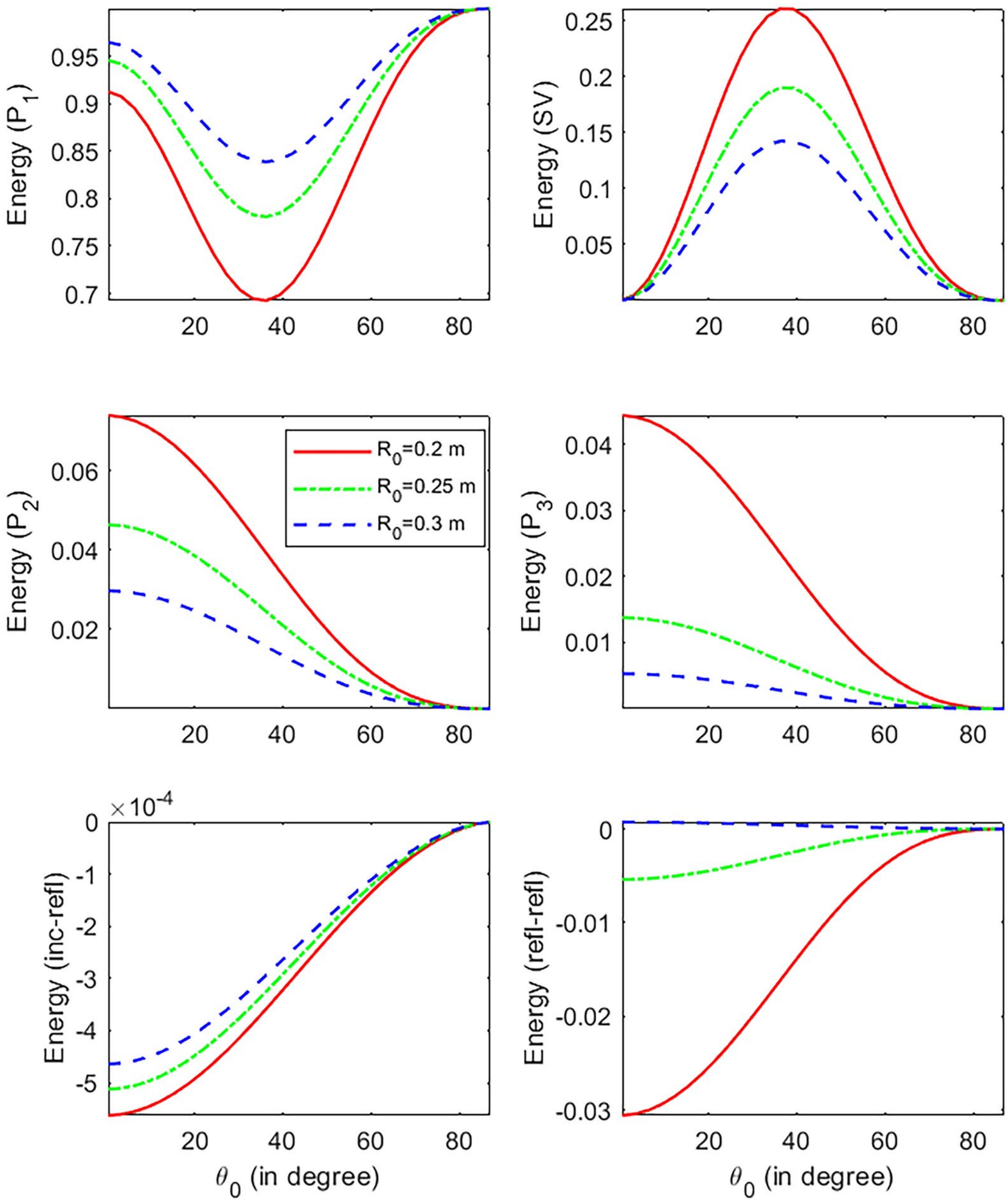

Fig. 5. Energy shares as a function of the incidence direction (θ_0) with different inclusion radius (incident P_1 wave).

as the angle of incidence rises. Wave P_3 has minimal impact on the fluid flow induced. It is seen that the fluid flow that is produced by waves P_2 and P_3 diminishes when the incidence gets closer to the direction of grazing. On the other hand, the fluid flow caused by the P_1 wave may be detected at both normal and grazing incidence temperatures. Each factor considerably impacted the wave-induced fluid flow when taken together.

SV-wave incidence
Following this, we will analyze the occurrence of the *SV* wave. The WIFF is affected by porosity (ϕ), water saturation (S_2), and inclusion radius (R_0), as can be seen in Figs. 15, 16 and 17. This is comparable to the situation shown in Figures 12, 13 and 14, which depicts the incident wave P_1. As can be observed in the case of the incident wave P_1, these properties also influence WIFF, which is analogous. However, when compared to the incident P_1 wave, the influence of the incident direction on WIFF is not comparable. When the waves strike the surface at normal and grazing angles, the fluid flow created by these waves is no longer there. Waves P_1 and P_2 are the key elements that influence fluid flow, and the scenario is quite similar to the one with the incident wave. However, when the wave is incident at a grazing angle, it does not contribute to the WIFF. Except for the normal and grazing angles, the P_2 wave contributes to the WIFF over the whole spectrum of incidence angles.

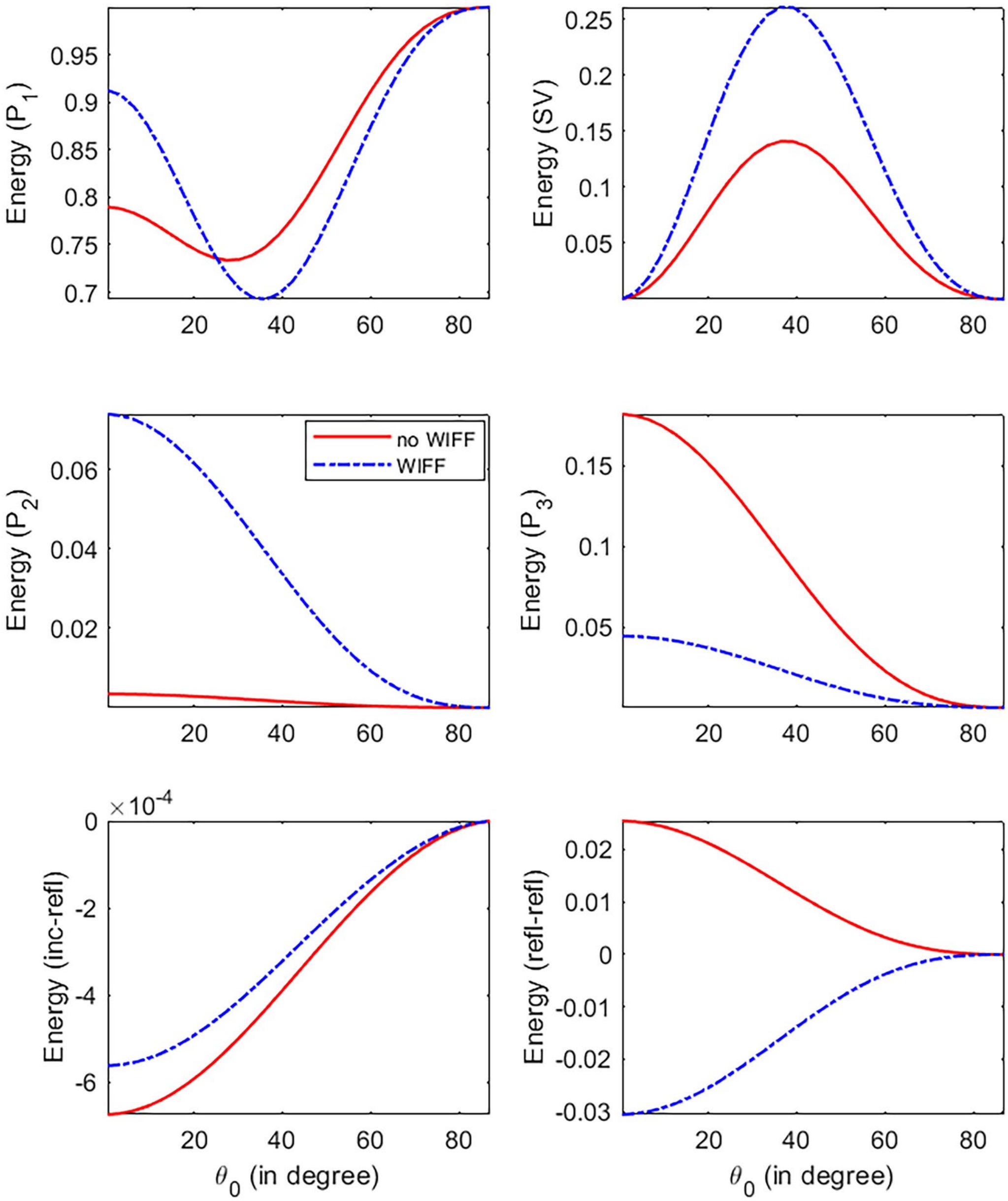

Fig. 6. Energy shares as a function of the incidence direction (θ_0) in the presence and absence of WIFF (incident P_1 wave).

Conclusions

The purpose of this study is to evaluate the characteristics of wave-induced fluid flow (WIFF) in unsaturated porous media, as well as the properties of the seismic waves that are reflected. An eigensystem is generated, and the Christoffel equations clarify the existence of three longitudinal waves and one transverse wave within the medium, along with their propagation characteristics. The porous media is considered dissipative due to the viscosities present in the saturated fluids. The incident and reflected waves are classified as inhomogeneous waves due to the dissipative nature of the medium. We calculate the poroelastic reflection coefficients for every angle of incidence at the boundary surface of sealed pores in the porous media. Subsequently, these poroelastic reflection coefficients are used to compute the fluid flow induced by the longitudinal waves. Additionally, we calculate the distribution of incident energy among the reflected waves at the boundary of the reflecting medium. From the numerical example, several findings emerge that are insightful and relevant, as listed below.

i. No critical angle is observed when a faster dilatational wave strikes the surface. In contrast, a critical angle is noted whenever a shear wave encounters a stress-free surface.
ii. The graphical representations of bulk energy shares associated with various reflected waves clearly demonstrate that, for both normal and grazing incidences, only one type of reflected wave physically persists among all the reflected waves. This type of reflected wave is identical to the incident wave.

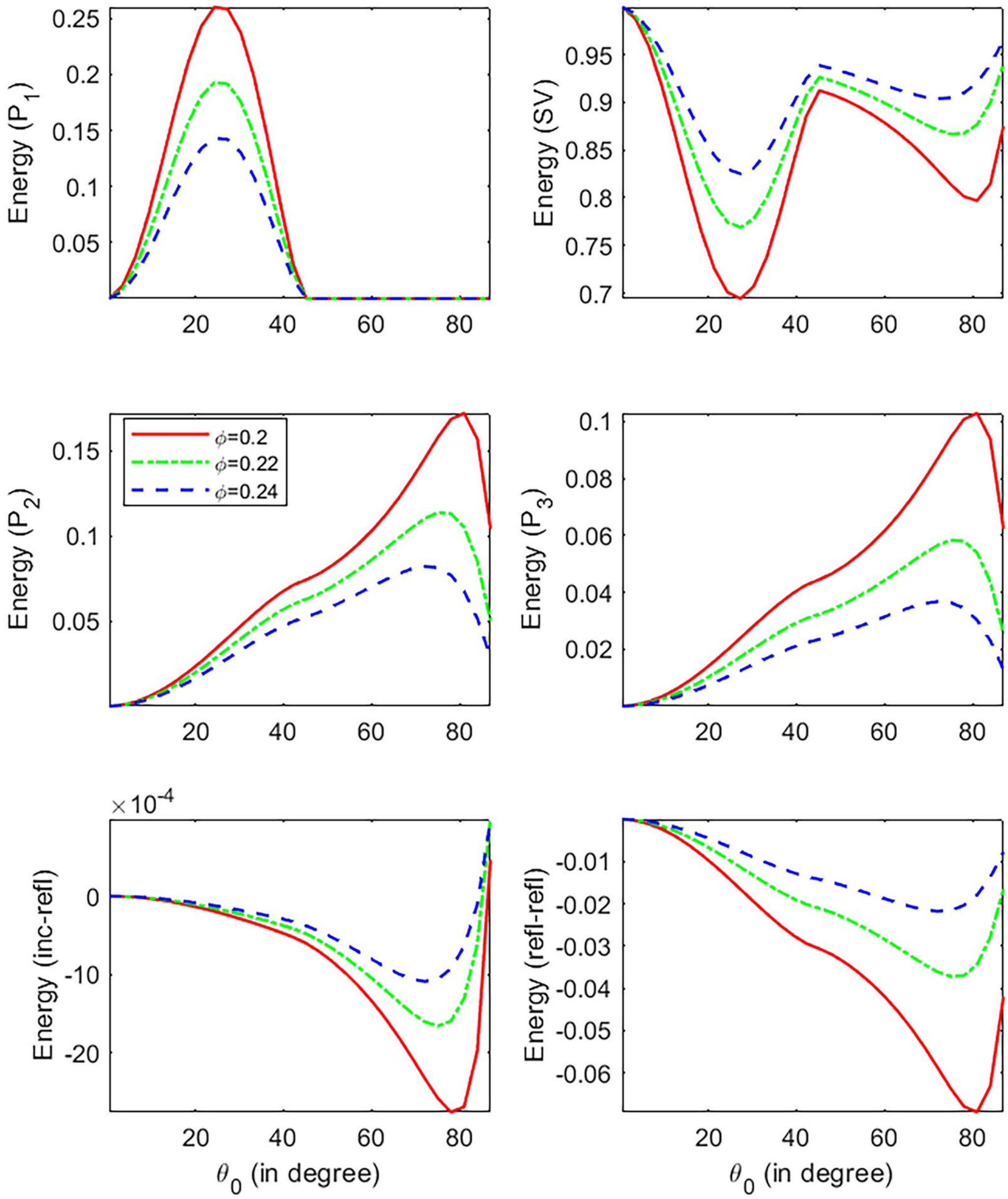

Fig. 7. Energy shares as a function of the incidence direction (θ_0) with different porosity (incident *SV* wave).

iii. The energy shares associated with distinct energy types are functions of incident direction, water saturation, porosity, inclusion radius, WIFF, and wave frequency.
iv. For the incidence of the $P_1(SV)$ wave, an increase in porosity and inclusion radius strengthens (weakens) the reflected P_1 wave but weakens (strengthens) the refracted *SV* wave. Other reflected waves may weaken slightly with the increase in porosity and inclusion radius in both cases.
v. For the incidence of the $P_1(SV)$ wave, an increase in water saturation weakens (strengthens) the reflected P_1 wave but strengthens (weakens) the refracted *SV* wave. Other reflected waves may strengthen slightly with the increase in water saturation in both cases.
vi. The increase in wave frequency weakens the reflected P_2 wave for both incident waves. In contrast, all other refracted waves may strengthen with the increase in frequency.
vii. The energy partition remains unchanged near grazing incidence for longitudinal waves despite variations in porosity, inclusion radius, water saturation, and frequency for the incidence of the P_1 wave. In contrast, the *SV* wave is unaffected at both normal and grazing incidences.
viii. It has been demonstrated that the conservation law for incident energy is upheld at all angles of incidence during the reflection process. To accurately account for the distribution of energy among the various reflected waves, it is essential to consider the energy dissipated during the interference process that occurs between different pairs of waves in the dissipative medium. This further substantiates the correctness of the numerical calculations from an analytical perspective.

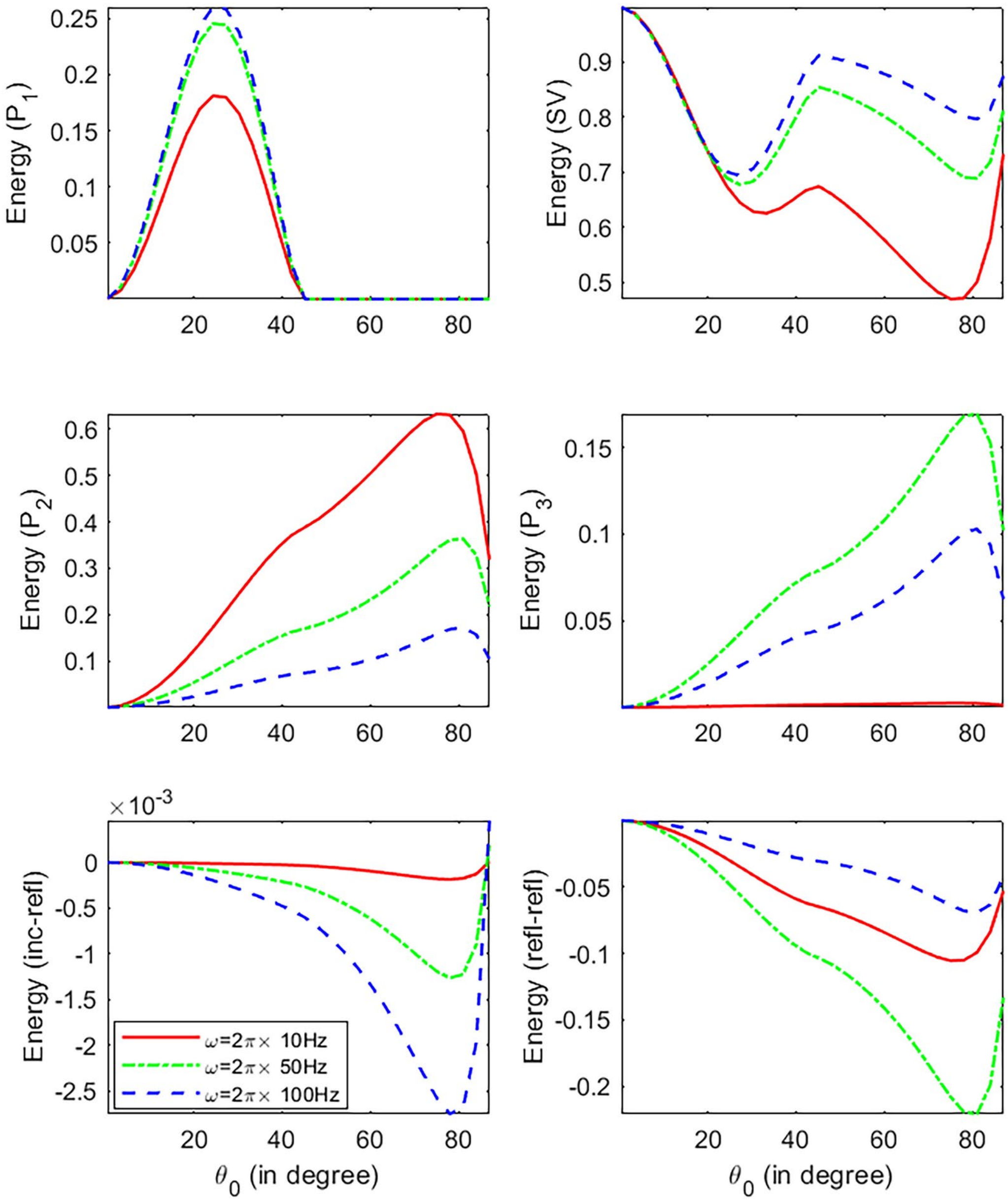

Fig. 8. Energy shares as a function of the incidence direction (θ_0) with different frequency (incident *SV* wave).

ix. For the incidence of the P_1 (SV) wave, the reflected SV (P_1) wave is amplified across the entire range of incident directions in the presence of WIFF. A similar behavior is observed for the P_2 and P_3 waves in the presence of WIFF for both incident waves (i.e., P_1 and *SV*).

x. The P_1 and P_2 waves significantly contribute to WIFF for both types of incidence (i.e., P_1 and *SV* incidence). The faster wave, P_1, contributes to WIFF at both grazing and normal incidences when the P_1 wave is incident. In contrast, the slower waves do not contribute at grazing incidence. However, none of the waves contribute to WIFF at either grazing or normal incidences in the case of an incident *SV* wave.

In practical applications, the petroleum industry commonly employs seismic reflection techniques to investigate sedimentary basins for hydrocarbon-trapping structures. This method is utilized to explore water, oil, and gas resources. Additionally, the location of high-saturation areas can be identified through the analysis of reflected seismic waves. In today's world, water, oil, and gas are essential to our daily lives; without them, our existence would be significantly challenged. The seismic reflection technique provides valuable structural information and has become the primary strategy for conducting comprehensive investigations of the deep crust. The model under evaluation represents a realistic scenario that may arise during the search for water or hydrocarbons. The search methodologies utilizing WIFF may yield significant insights into the reservoir's productivity. Therefore, the authors believe that researchers in structural engineering and exploration may be inclined to adopt the proposed model in their simulation studies.

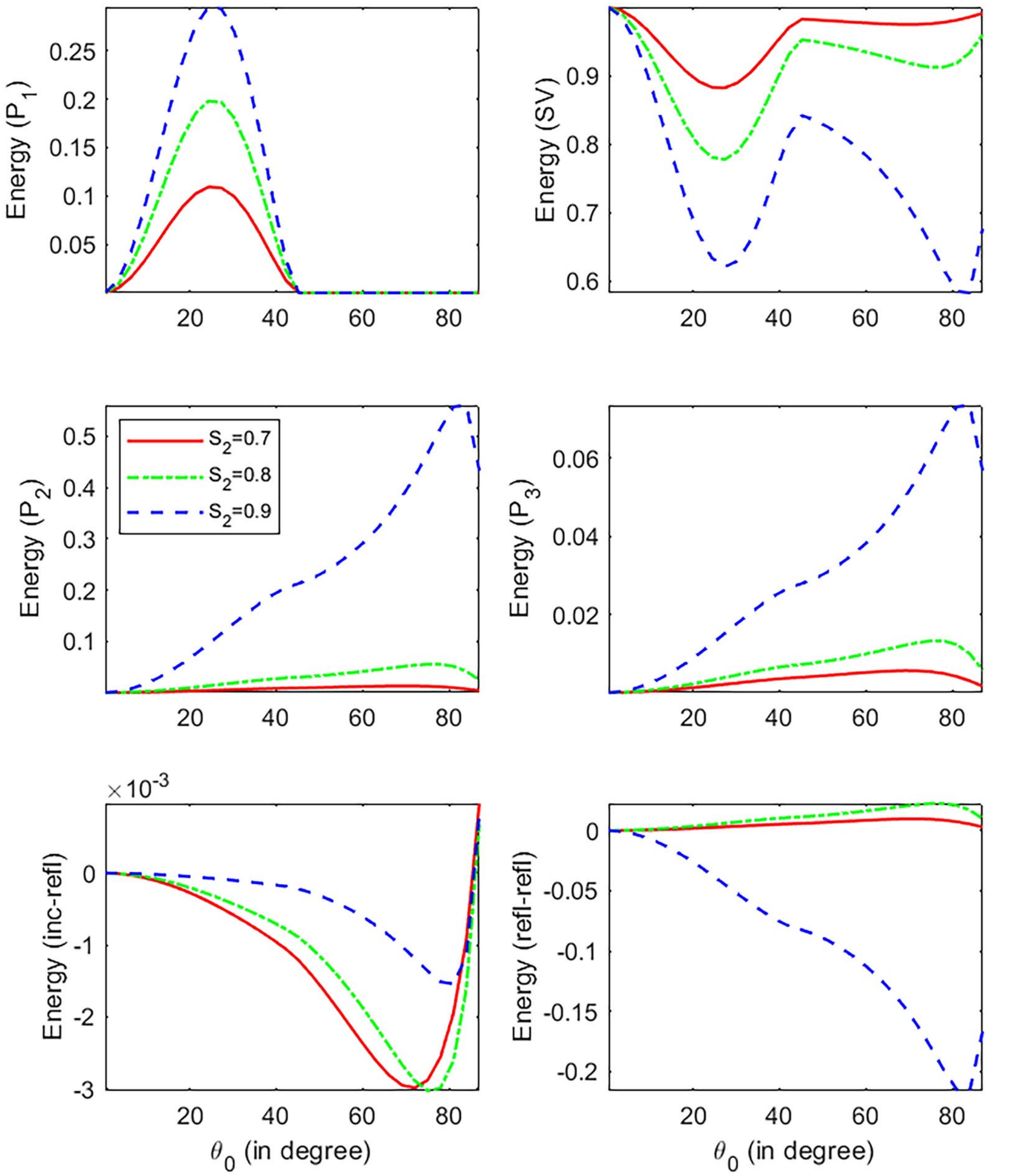

Fig. 9. Energy shares as a function of the incidence direction (θ_0) with different water saturation (incident *SV* wave).

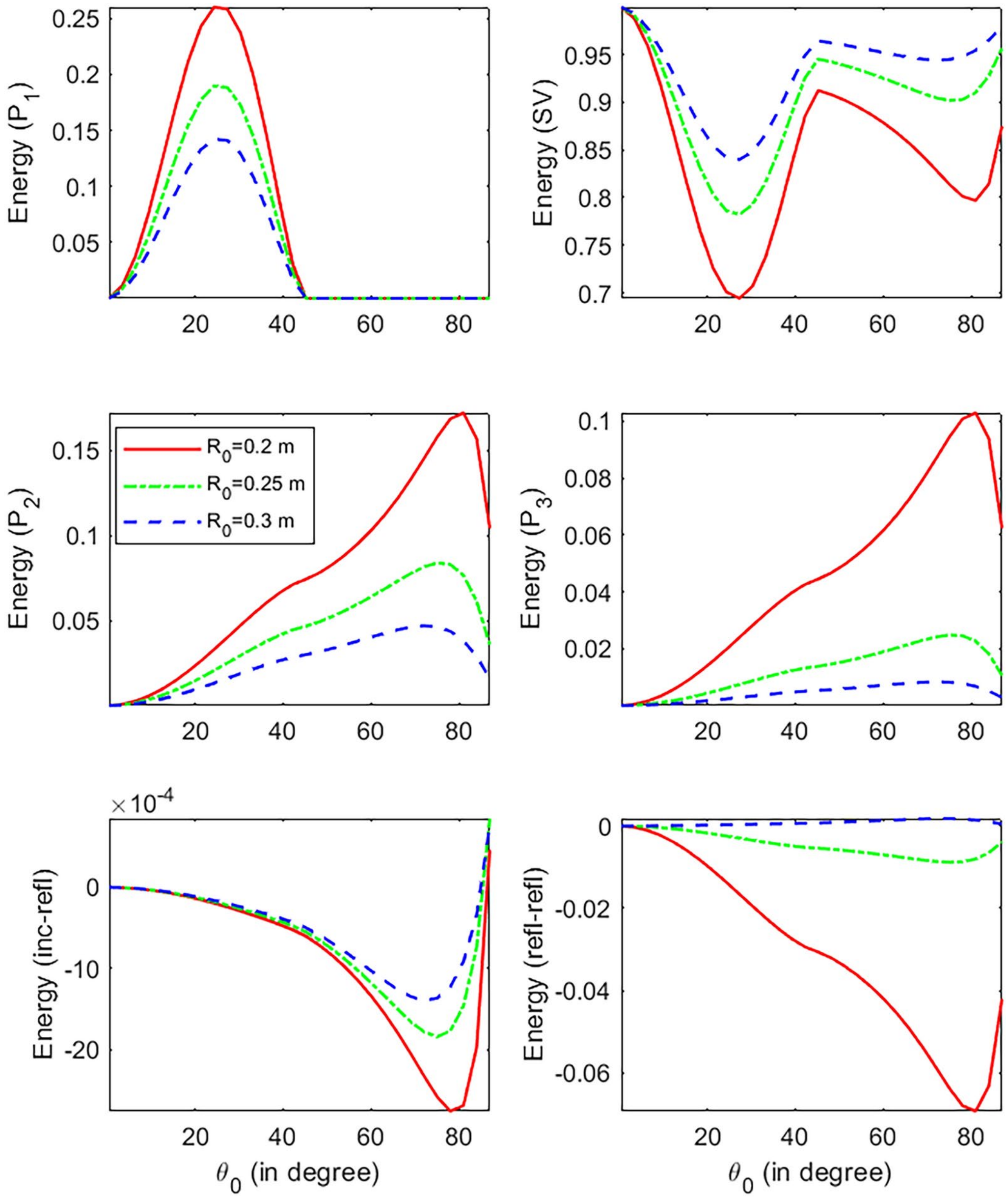

Fig. 10. Energy shares as a function of the incidence direction (θ_0) with different inclusion radius (incident *SV* wave).

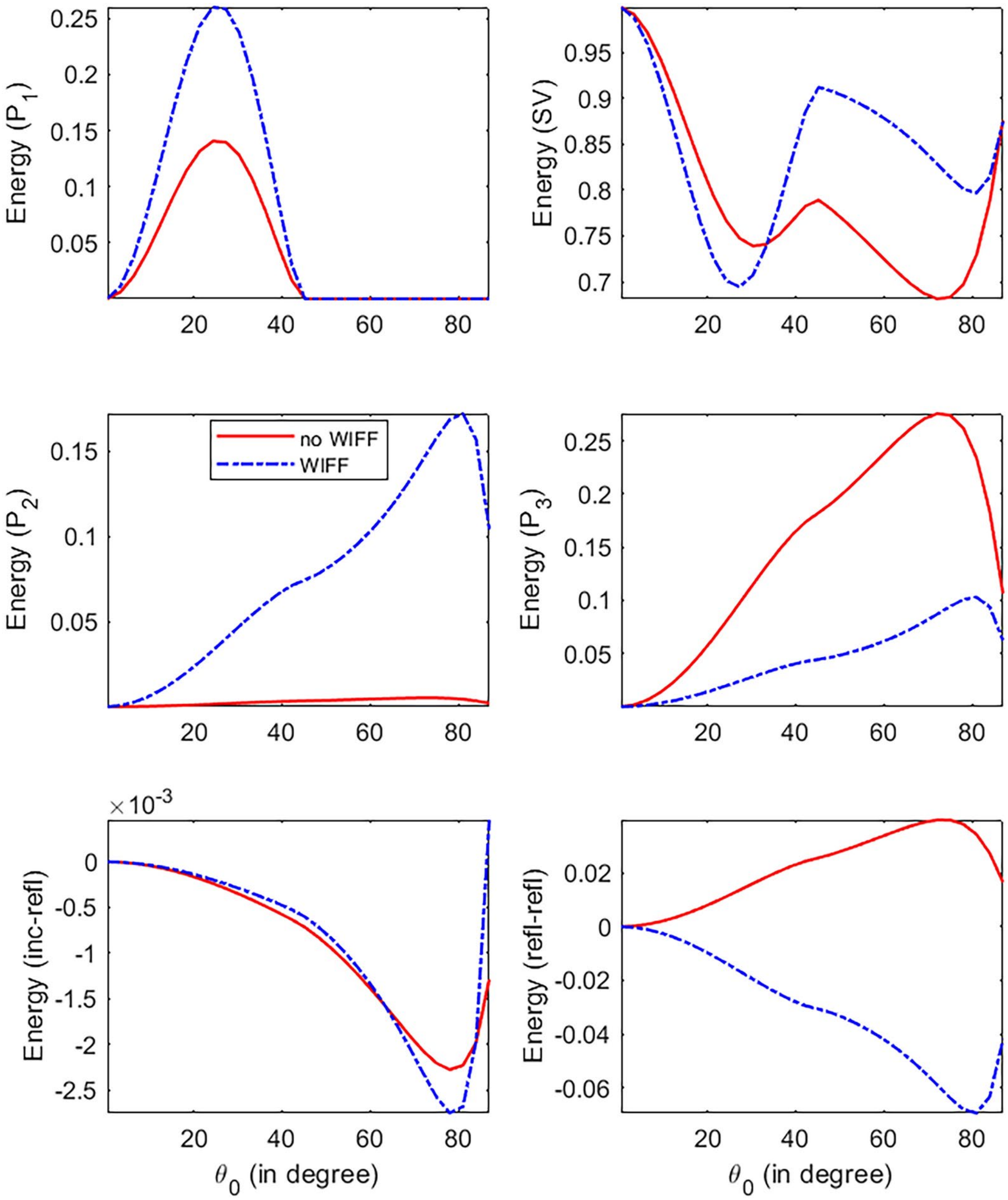

Fig. 11. Energy shares as a function of the incidence direction (θ_0) in the presence and absence of WIFF (incident P_1 wave).

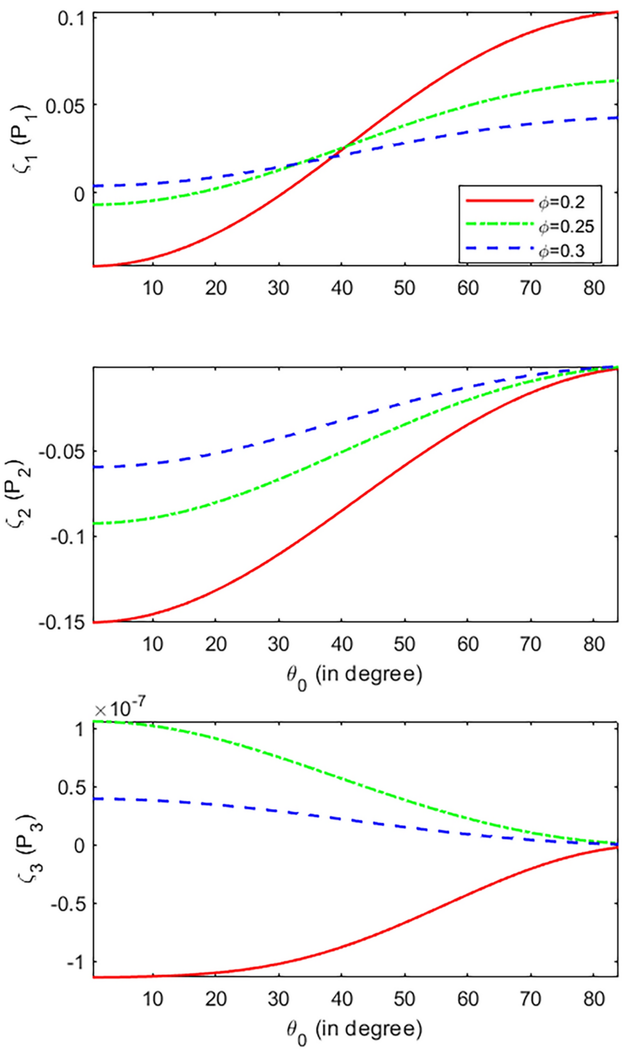

Fig. 12. WIFF as a function of the incidence direction (θ_0) with different porosity (incident P_1 wave).

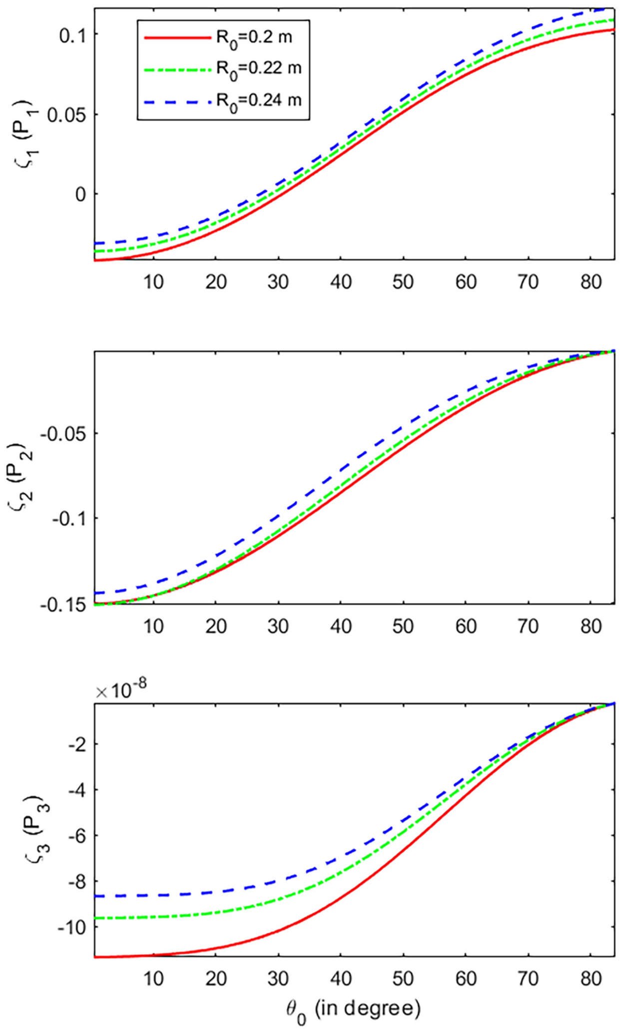

Fig. 13. WIFF as a function of the incidence direction (θ_0) with different inclusion radius (incident P_1 wave).

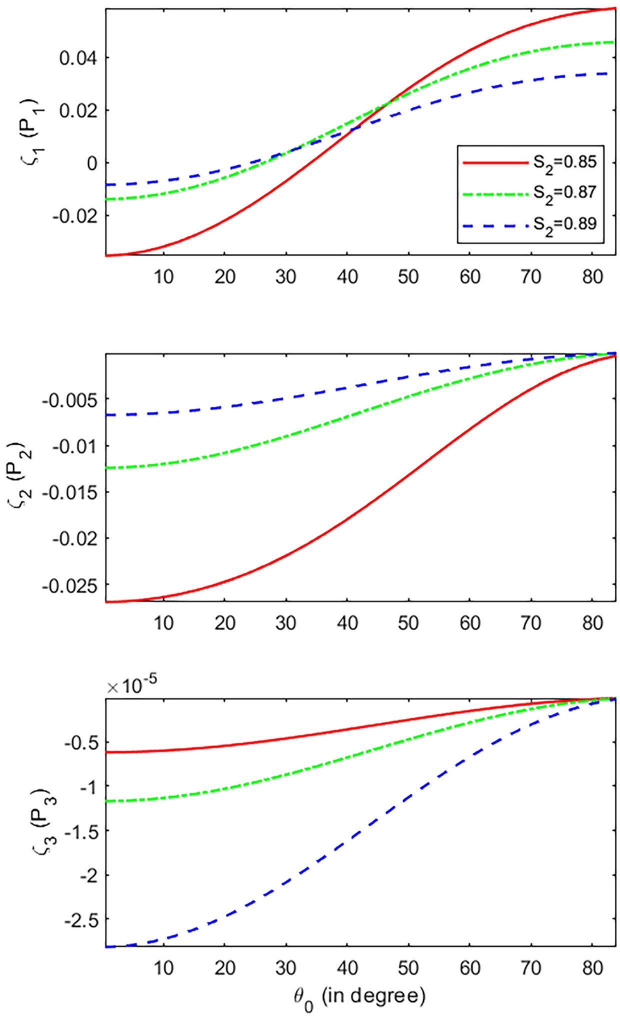

Fig. 14. WIFF as a function of the incidence direction (θ_0) with different water saturation (incident P_1 wave).

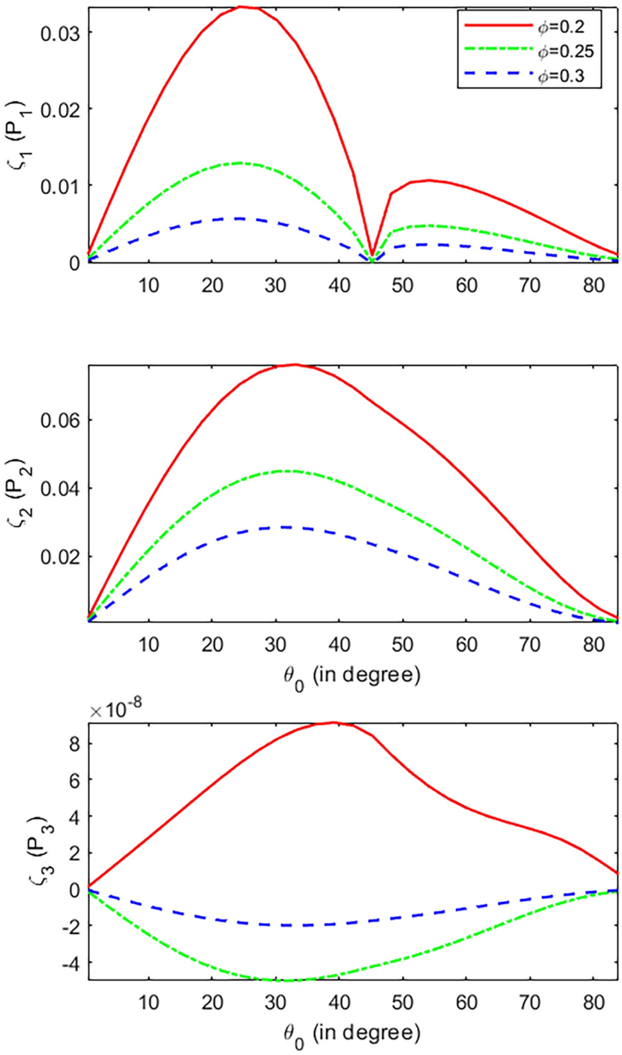

Fig. 15. WIFF as a function of the incidence direction (θ_0) with different porosity (incident *SV* wave).

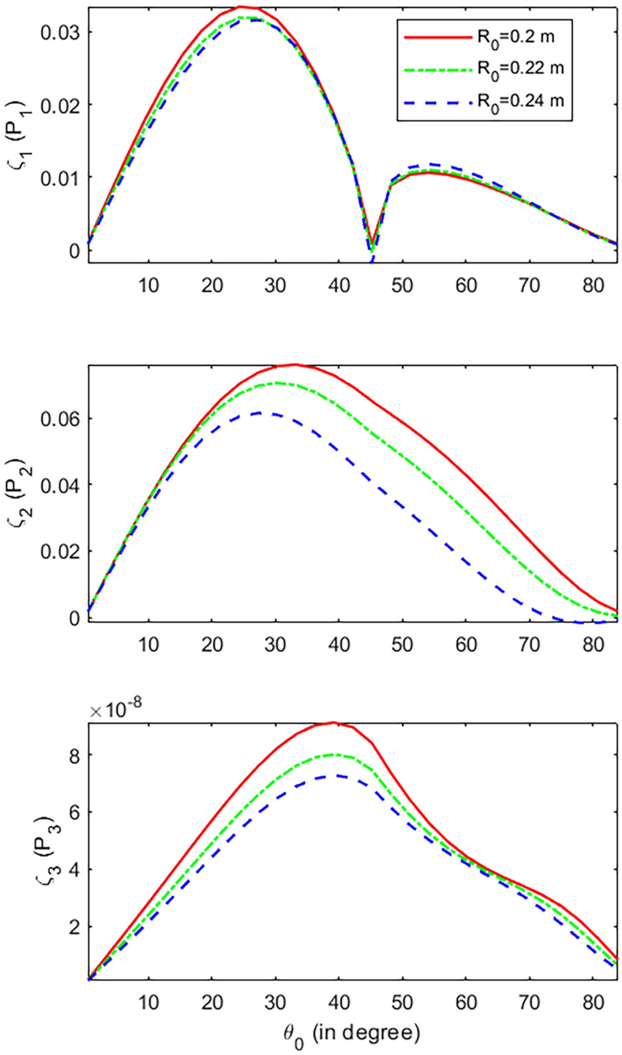

Fig. 16. WIFF as a function of the incidence direction (θ_0) with different inclusion radius (incident *SV* wave).

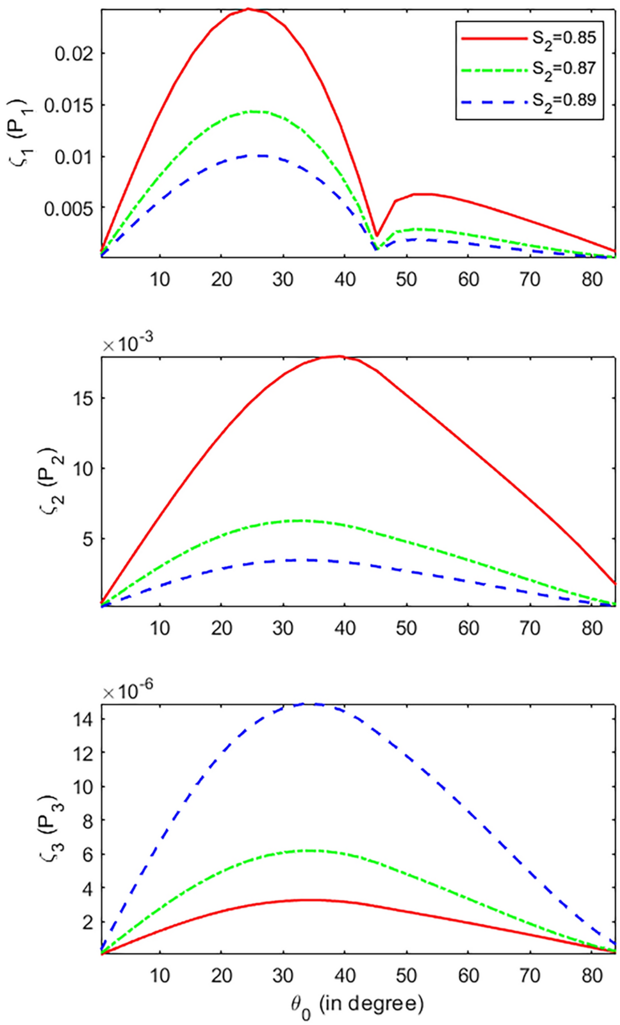

Fig. 17. WIFF as a function of the incidence direction (θ_0) with different water saturation (incident *SV* wave).

Data availability
The datasets used and/or analyzed during the current study available from the corresponding author on reasonable request.

Received: 6 October 2024; Accepted: 3 April 2025
Published online: 29 May 2025

References
1. Biot, M.A. Theory of propagation of elastic waves in a fluid-saturated porous solid. I. Low frequency range. *J. Acoust. Soc. Am.* **28**(2), 168–178 (1956).
2. Biot, M.A. Theory of propagation of elastic waves in a fluid-saturated porous solid. II. Higher frequency range. *J. Acoust. Soc. Am.* **28**(2), 179–191 (1956).
3. Biot, M.A. Mechanics of deformation and acoustic propagation in porous media. *J. Appl. Phys.* **33**(4), 1482–1498 (1962).
4. Gassmann, F. Elastic waves through a packing of spheres. *Geophysics* **16**(4), 673–685 (1951).
5. Pride, S.R., Gangi, A.F. & Morgan, F.D. Deriving the equations of motion for porous isotropic media. *J. Acoust. Soc. Am.* **92**(6), 3278–3290 (1992).
6. Lévy, Thérese. Propagation of waves in a fluid-saturated porous elastic solid. *Int. J. Eng. Sci.* **17**(9), 1005–1014 (1979).
7. Auriault, J. L. Dynamic behaviour of a porous medium saturated by a newtonian fluid. *IInt. J. Eng. Sci.* **18**(6), 775–785 (1980).
8. Burridge, Robert & Keller, Joseph B. Poroelasticity equations derived from microstructure. *J. Acoust. Soc. Am.* **70**(4), 1140–1146 (1981).
9. Harish Babu, D. et al. Numerical and neural network approaches to heat transfer flow in mhd dissipative ternary fluid through darcy-forchheimer permeable channel. *Case Stud. Therm. Eng.* **60**, 104777 (2024).
10. Zhao, X. et al. Analysis of free convective flow of nanofluid due to inclined surface with thermos-diffusion effects and chemical reaction. *Tribol. Int.* **197**, 109792 (2024).
11. Kommaddi, H.B., Kodi, R., Ganteda, C. & Lorenzini, G. Heat and mass transfer on unsteady mhd chemically reacting rotating flow of jeffrey fluid past an inclined plates under the impact of hall current, diffusion thermo and radiation absorption. *J. Adv. Res. Fluid Mech. Therm. Sci.* **111**(2), 225–241 (2023).
12. Kodi, R., Mopuri, O., Sree, S. & Konduru, V. Investigation of mhd casson fluid flow past a vertical porous plate under the influence of thermal diffusion and chemical reaction. *Heat Transfer* **51**(1), 377–394 (2022).
13. Raghunath, K., Obulesu, M. & Raju, K.V. Radiation absorption on mhd free conduction flow through porous medium over an unbounded vertical plate with heat source. *Int. J. Ambient Energy* **44**(1), 1712–1720 (2023).
14. Bear, J. *Dynamics of Fluids in Porous Media*. (Courier Corporation, 1988).
15. Brutsaert, W. The propagation of elastic waves in unconsolidated unsaturated granular mediums. *J. Geophys. Res.* **69**(2), 243–257 (1964).
16. Brutsaert, W. & Luthin, J.N. The velocity of sound in soils near the surface as a function of the moisture content. *J. Geophys. Res.* **69**(4), 643–652 (1964).
17. Bedford, A. & Drumheller, D. S. Theories of immiscible and structured mixtures. *Int. J. Eng. Sci.* **21**(8), 863–960 (1983).
18. Garg, S. K. & Nayfeh, A. H. Compressional wave propagation in liquid and/or gas saturated elastic porous media. *J. Appl. Phys.* **60**(9), 3045–3055 (1986).
19. Berryman, J.G., Thigpen, L. & Chin, R.C.Y. Bulk elastic wave propagation in partially saturated porous solids. *J. Acoust. Soc. Am.* **84**(1), 360–373 (1988).
20. Santos, J.E., Jim Douglas, Jr, Corberó, J. & Lovera, O.M. A model for wave propagation in a porous medium saturated by a two-phase fluid. *J. Acoust. Soc. Am.* **87**(4), 1439–1448 (1990).
21. Santos, J.E., Corberó, J.M. & Jim Douglas, Jr. Static and dynamic behavior of a porous solid saturated by a two-phase fluid. *J. Acoust. Soc. Am.* **87**(4), 1428–1438 (1990).
22. Corapcioglu, M.Y. & Tuncay, K. Propagation of waves in porous media. In *Advances in Porous Media*. Vol. 3. 361–440. (Elsevier, 1996).
23. Tuncay, K. & Corapcioglu, M.Y. *Wave Propagation in Poroelastic Media Saturated by Two Fluids*. (1997).
24. Wei, C. & Muraleetharan, K.K. A continuum theory of porous media saturated by multiple immiscible fluids: I. Linear poroelasticity. *Int. J. Eng. Sci.* **40**(16), 1807–1833 (2002).
25. Wei, C. A continuum theory of porous media saturated by multiple immiscible fluids: II. Lagrangian description and variational structure. *Int. J. Eng. Sci.* **40**(16), 1835–1854 (2002).
26. Hanyga, Andrzej. Two-fluid porous flow in a single temperature approximation. *Int. J. Eng. Sci.* **42**(13–14), 1521–1545 (2004).
27. Jian-Fei, L. & Hanyga, A. Linear dynamic model for porous media saturated by two immiscible fluids. *Int. J. Solids Struct.* **42**(9–10), 2689–2709 (2005).
28. Lo, W.-C. Propagation and attenuation of rayleigh waves in a semi-infinite unsaturated poroelastic medium. *Adv. Water Resour.* **31**(10), 1399–1410 (2008).
29. Lo, W.-C., Sposito, G. & Majer, E. Wave propagation through elastic porous media containing two immiscible fluids. *Water Resour. Res* **41**(2) (2005).
30. Lo, W.-C., Sposito, G. & Majer, E. Analytical decoupling of poroelasticity equations for acoustic-wave propagation and attenuation in a porous medium containing two immiscible fluids. *J. Eng. Math.* **64**, 219–235 (2009).
31. Lo, W.-C., Sposito, G., Majer, E. & Yeh, C.-L. Motional modes of dilatational waves in elastic porous media containing two immiscible fluids. *Adv. Water Resour.* **33**(3), 304–311 (2010).
32. Lo, W.-C., Yeh, C.-L. & Lee, J.-W. Effect of viscous cross coupling between two immiscible fluids on elastic wave propagation and attenuation in unsaturated porous media. *Adv. Water Resour.* **83**, 207–222 (2015).
33. Arora, A., Painuly, A. & Tomar, S.K. Body waves in composite solid matrix containing two immiscible fluids. *Transport Porous Media* **108**, 531–554 (2015).
34. Xiong, F., Liu, J., Guo, Z. & Liu, J. Wave equations of porous media saturated with two immiscible fluids based on the volume averaging method. *Front. Earth Sci.* **9**, 618909 (2021).
35. Wang, E., Carcione, J.M, & Ba, J. Wave simulation in partially saturated porothermoelastic media. *IEEE Trans. Geosci. Remote Sens.* **60**, 1–14 (2021).
36. Sun, W. On the theory of biot-patchy-squirt mechanism for wave propagation in partially saturated double-porosity medium. *Phys. Fluids* **33**(7) (2021).
37. Solazzi, S.G., Damien Jougnot, J., Rubino, G. & Holliger, K. Dynamic relative permeabilities for partially saturated porous media accounting for viscous coupling effects: An analytical solution. *Transport Porous Media* **147**(3), 653–677 (2023).
38. Deng, T. et al. Numerical modeling of seismic wave propagation in loosely deposited partially saturated sands: An application to a mine dump monitoring case. *Environ. Earth Sci.* **82**(9), 200 (2023).
39. Santos, J. E., Savioli, G. B. & Ba, J. Analysis of wave propagation in non-isothermal poroelastic solids saturated by two-phase fluids. *Geophys. J. Int.* **237**(2), 1030–1047 (2024).

40. Yao, Q., Han, D., Yan, F. & Zhao, L. Modeling attenuation and dispersion in porous heterogeneous rocks with dynamic fluid modulus. *Geophysics* **80**(3), D183–D194 (2015).
41. Müller, T.M., Gurevich, B. & Lebedev, M. Seismic wave attenuation and dispersion resulting from wave-induced flow in porous rocks-A review. *Geophysics* **75**(5), 75A147-75A164 (2010).
42. Quintal, B., Schmalholz, S.M., & Podladchikov, Y.Y. Impact of fluid saturation on the reflection coefficient of a poroelastic layer. *Geophysics* **76**(2), N1–N12 (2011).
43. Khalid, P. & Ahmed, N. Modulus defect, velocity dispersion and attenuation in partially-saturated reservoirs of jurassic sandstone, Indus Basin, Pakistan. *Stud. Geophys. Geodaet.* **60**, 112–129 (2016).
44. Shi, Z., He, X., Chen, D. & Wang, X. Seismic wave dispersion and attenuation resulting from multiscale wave-induced fluid flow in partially saturated porous media. *Geophys. J. Int.* **236**(2), 1172–1182 (2024).
45. Borcherdt, R.D. Reflection-refraction of general p-and type-i s-waves in elastic and anelastic solids. *Geophys. J. Int.* **70**(3), 621–638 (1982).
46. Achenbach, J. D. *Wave Propagation in Elastic Solids* (North-Holland, 1973).
47. Krebes, E. S. The viscoelastic reflection/transmission problem: Two special cases. *Bull. Seismol. Soc. Am.* **73**(6A), 1673–1683 (1983).
48. Ainslie, M.A. & Burns, P.W. Energy-conserving reflection and transmission coefficients for a solid-solid boundary. *J. Acoust. Soc. Am.* **98**(5), 2836–2840 (1995).
49. Yang, J. & Sato, T. Effects of pore-water saturation on seismic reflection and transmission from a boundary of porous soils. *Bull. Seismol. Soc. Am.* **90**(5), 1313–1317 (2000).

Author contributions
Manjeet Kumari, Pradeep Kaswan, Manjeet Kumar: Conceptualization, Methodology, Software, Visualization, Investigation, Writing- Original draft preparation. Roland W Lewis, Hakan F. OZTOP, Nirmal Singh: Data curation, Validation, Supervision, Resources, Writing - Review & Editing. Adebowale Martins Obalalu, Mukesh Pushkarna, Milkias Berhanu: Project administration, Supervision, Resources, Writing - Review & Editing.

Competing interests
The authors declare no competing interests.

Additional information
Supplementary Information The online version contains supplementary material available at https://doi.org/10.1038/s41598-025-97275-x.

Correspondence and requests for materials should be addressed to M.B.

Reprints and permissions information is available at www.nature.com/reprints.

Publisher's note Springer Nature remains neutral with regard to jurisdictional claims in published maps and institutional affiliations.